

Competing automorphisms and disordered Floquet codes

Cory T. Aitchison¹ and Benjamin Béri^{1,2}

¹*DAMTP, University of Cambridge, Wilberforce Road, Cambridge, CB3 0WA, UK*

²*T.C.M. Group, Cavendish Laboratory, University of Cambridge, J.J. Thomson Avenue, Cambridge, CB3 0HE, UK*

Topological order is a promising basis for quantum error correction, a key milestone towards large-scale quantum computing. Floquet codes provide a dynamical scheme for this while also exhibiting Floquet-enriched topological order (FET) where anyons periodically undergo a measurement-induced automorphism that acts uniformly in space. We study deformed Floquet codes where automorphisms have a spatiotemporally heterogeneous distribution—the automorphisms “compete”. We characterize the effect of this competition on Abelian-anyon FETs, showing how the evolution and loss of logical information are linked to the anyons that are invariant under the automorphisms’ transition map or that localize at their boundaries. We present an example microscopic realization of this behavior using disorder in the dynamic automorphism color code. This naturally leads to a description of the space of its FETs, which we characterize by establishing when parameter-space paths connecting distinct FETs can preserve logical information. We also show that transitions between distinct FETs display criticality described by bond percolation. The perspective of competing automorphisms captures essential features of possible FETs and their transitions, and may elucidate key mechanisms involving topological order, automorphisms, and disorder.

I. INTRODUCTION

Quantum error-correcting (QEC) codes are crucial for the effective, scalable operation of current and future quantum computers [1–9]. These codes envision a smaller number of protected logical qubits encoded within a larger Hilbert space of physical qubits. In a similar vein, quantum systems with long-range entanglement—exhibiting topological order (TO)—display robustness to local perturbations, host excitations with fractional statistics known as anyons, and support a topology-dependent ground-state degeneracy [10, 11]. Because of their inherent robustness, TO systems are promising candidates for QEC codes.

These topological QEC codes have historically been static: the code properties, such as the stabilizer group in stabilizer codes [2, 12], are fixed through time. A recent class of codes, so-called dynamical codes, on the other hand forgo this notion. They are inherently time-evolving and this can improve code properties or enable novel behaviors [13–15]. The first such example was the honeycomb code [16], a form of dynamical code called a Floquet code due to its time-periodic evolution. By measuring only two-qubit Pauli operators in a particular sequence, a stabilizer group emerges that enables the detection and correction of errors. Each stage in the sequence generates a TO equivalent to a static toric code (TC) [17–20]. Since its introduction, studies of the honeycomb code also included its boundaries [21, 22] and lattice defects [23]. Other dynamical codes have also been proposed, such as the CSS honeycomb code [14, 24], the automorphism code [25], the dynamic automorphism color code [26], the $x+y$ Floquet code [27], the XYZ ruby code [28], $(3+1)$ D Floquet codes [29], or the hyperbolic Floquet code [30]. Theoretical studies of dynamical codes include perspectives such as subsystem codes [14, 31], quantum cellular automata [32], twist-defect networks [33], adiabatic paths of Hamiltonians [25], or fixed-

point path integrals [34–37], and aspects of Floquet code phenomenology were also linked to symmetry topological field theory [38].

A key property of the honeycomb code is its period doubling of expectation values: while the period of the measurement sequence is 3, the TO takes 6 stages to return to its original state. Specifically, two of the TC anyons, labeled \mathbf{e} and \mathbf{m} , interchange every measurement period. These permutations correspond to bijective structure-preserving mappings, or automorphisms. Periodic implementations of such automorphisms extend topological order into a Floquet-like phase [25]. This Floquet-enriched topological order (FET) arises not only within dynamical codes, but was originally proposed for driven $(2+1)$ D TO systems [39, 40].

An important question is whether these FETs are robust against disorder. For the honeycomb code, recent results suggest competitive levels of tolerance to fabrication defects on realistic physical devices [41, 42], and that its FET persists amid random modifications to the measurement sequence, such as omitting or splitting up the two-qubit Pauli operators [43, 44]. Characterizing the effects of disorder in more general FETs is however an open question, which is part of our goal in this work. As we will show, such disordered FETs can have rich phenomenology and form a new part of the landscape of quantum matter emerging from disordered measurements [44–61].

In this work we study FETs with disorder and establish general features that hold for any underlying Abelian TO. To this end, we introduce a picture of “competing automorphisms”: TO systems where automorphisms are spatiotemporally heterogeneous, i.e., multiple automorphisms arise concurrently and act on different disjoint subregions of the manifold every period. We characterize these competing automorphisms by determining their effect on the evolution of and measurements affecting the dynamical code space. These behaviors are fundamentally decided by the homology of boundary segments of

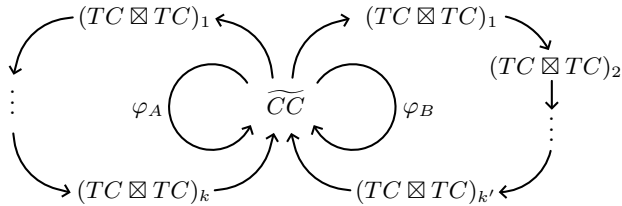


Figure 1. A color code topological order (\widetilde{CC}) can be mapped through a series of doubled toric code topological orders ($TC \boxtimes TC$) via anyon condensation. Upon returning to the original \widetilde{CC} , an automorphism φ_A permutes the anyons of the model, creating a Floquet-enriched topological order (FET). We use disorder to modify the condensation sequence by adding or removing a condensation. Returning to \widetilde{CC} may now result in a different automorphism, φ_B , and a different FET.

the automorphisms’ domain walls, and the anyons that localize at or are invariant under the transition maps of the competing automorphisms.

This picture helps characterize dynamical codes subjected to disorder. We present an example microscopic model that realizes such competing automorphisms using the dynamic automorphism (DA) color code [26]. In this code, different measurement sequences result in different automorphisms via anyon condensation [24, 62–67], cf. Fig. 1. Whereas the TC TO of the honeycomb code supports only an automorphism group isomorphic to the 2-element symmetry group S_2 , the DA color code is based on a color code (CC) TO with a 72-element automorphism group [68–71]. This is a wide range of automorphisms that can compete in the presence of disorder, which we introduce by randomly and independently missing or including measurements.

We study how these competing automorphisms shape the topology of the space of potential color code FETs. We formulate necessary and sufficient conditions for different FETs to be connected (i.e., there to be a sequence of parameter-space paths between them, with each path formed by modifying their measurement sequences as in Fig. 1), or for them to be “logically-connected” (i.e., a consistent logical subspace to be protected along each path of the sequence and over multiple periods). Performing numerical simulations, we establish phase diagrams for these disorder models and show that they exhibit critical behavior described by bond percolation. Our study thus explores what new features arise in dynamical TOs, while also investigating the robustness of the DA color code to disordered measurements. Our approach is generalizable to other dynamical codes and TOs understandable through their automorphisms.

The rest of the paper is organized as follows: In Section II, we provide background on FETs and the DA color code. In Section III, we introduce competing automorphisms and characterize general features for any underlying

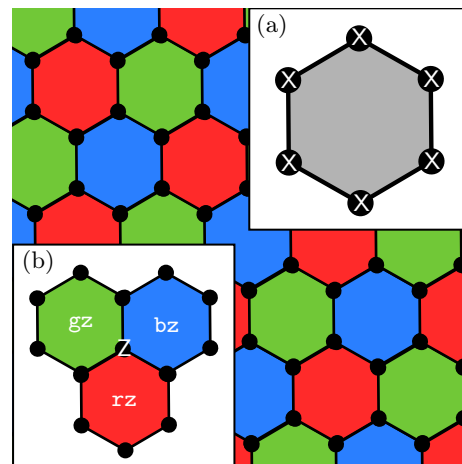


Figure 2. The 6-6-6 honeycomb lattice formed by hexagonal plaquettes, each assigned a color: red (r), green (g), or blue (b). Links are colored by their terminating plaquettes; a link connecting two red plaquettes is also red, for example. A qubit (black circle) occupies each lattice site. Inset (a). The weight-6 operator P_X constructed from single-qubit Pauli X terms, used in the Hamiltonian. Inset (b). A single-qubit Z excites bz , gz , and rz anyons in neighboring plaquettes.

ing Abelian TO. In Section IV we then propose a specific microscopic realization using a disordered DA color code and explore its features. We characterize the critical behavior of these models in Section V using analytic and numerical approaches. In Section VI we conclude and discuss some future directions.

II. BACKGROUND

The color code topological order (CC) is a quantum system defined on a 2D three-colorable lattice [68–71]. In our work, we focus on the 6-6-6 honeycomb lattice formed by tessellating hexagonal plaquettes shown in Fig. 2. We color each plaquette red (r), green (g), or blue (b) such that adjacent plaquettes are of different colors; a link that connects two plaquettes of the same color by convention adopts that color too. A qubit is placed on each lattice site and the Hamiltonian contains two species of commuting operators, P_X and P_Z , formed by the weight-6 Pauli X and Pauli Z tensor products on the corners of each hexagonal plaquette, with the identity elsewhere:

$$H_{CC} = - \sum_{\text{plaquette } p} P_{X,p} - \sum_{\text{plaquette } p} P_{Z,p}. \quad (1)$$

In the ground state of this Hamiltonian, a single-qubit Pauli operator at a lattice site excites three anyons in the three adjacent plaquettes, which we label by $c\sigma$ indicating both the hosting plaquette color $c \in \{r, g, b\}$ and the Pauli flavor $\sigma \in \{x, y, z\}$ that created it. A single-qubit X therefore creates rx , gx , and bx anyons, for example.

An \times applied to the two qubits of a red link creates a pair of \mathbf{rx} anyons on the plaquettes at its endpoints.

These anyons and their behavior fundamentally define a TO. Self-statistics capture the topological or spin-statistics of a particle, while the mutual statistics encode the Aharonov-Bohm phase of winding one anyon around another. In particular, bosons have trivial self-exchange statistics, fermions a -1 statistic, while (Abelian) anyons can accumulate a general phase in $SU(1)$. Mutual-semions accumulate a phase of -1 when braided. The vacuum particle, $\mathbf{1}$, is a boson and braids trivially with all other anyons. We have encountered already the 9 other nontrivial bosons of CC , formed by the combination of r, g, b colors and x, y, z flavors; two of these bosons that share the same color or flavor braid trivially, but otherwise are mutual-semions. There are also 6 fermions formed by multiple mutual-semions; these are listed in Appendix A. CC is isomorphic to two copies of TC , written as $CC \equiv TC \boxtimes TC$ denoting the external tensor product; any anyon in CC can be written as a tensor product of two anyons from TC [72–74].¹

The anyon theory of a TO is also characterized by fusion rules (whereby two anyons in proximity to each other are equivalent to a third) [75]. It is often convenient to represent the braiding and fusion rules of the color code by the “Mermin-Peres magic square” (hereafter referred to as the magic square) [76, 77]:

$$\begin{array}{c|c|c} \mathbf{rx} & \mathbf{ry} & \mathbf{rz} \\ \hline \mathbf{gx} & \mathbf{gy} & \mathbf{gz} \\ \hline \mathbf{bx} & \mathbf{by} & \mathbf{bz} \end{array} \quad (2)$$

such that bosons in the same row or column braid trivially while those that are not are mutual-semions. The fusion rules are such that two bosons in the same row or column fuse to make the third, and two anyons of the same type fuse (annihilate) to the vacuum. We write

$$\mathbf{rx} \times \mathbf{rz} = \mathbf{ry}, \quad \mathbf{rz} \times \mathbf{gz} = \mathbf{bz}, \quad \mathbf{gy} \times \mathbf{gy} = \mathbf{1}, \quad (3)$$

for example.

The automorphisms of a TO are maps between its anyon theories that preserve the statistics and fusion rules. For CC , these form a 72-element symmetry group $\text{Aut}[CC]$ that is in correspondence to a subgroup of the permutations of the magic square: $\text{Aut}[CC]$ can be decomposed² as $(S_3 \times S_3) \rtimes S_2$ such that we can write any automorphism as the product of one of $6 = 3!$ row or color permutations (the symmetry group S_3), 6 column or flavor permutations (S_3), and 2 color-flavor swapping reflections about the diagonal of the magic square (S_2) [26]. Appendix B provides a more detailed description of the

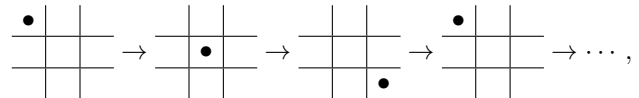
relevant group-theoretic concepts of the automorphism group; we summarize some key information here. We denote elements of $\text{Aut}[CC]$ using the cycle notation of the permutation group S_6 , indicating the transformation of the 6 anyon labels r, g, b , and x, y, z . Since all bosons are composed of one color and one flavor label, cycles must always be formed of either disjoint color and flavor cycles, or alternating color and flavor. $(rgx)(yz)$, for example, is not a member of $\text{Aut}[CC]$, but $(rx)(gy)(bz)$ and $(rg)(xyz)$ are. We write the identity map as id . Composition of two elements of $\text{Aut}[CC]$ are written as $\varphi_2\varphi_1$, evaluated as $(\varphi_2\varphi_1)(\mathbf{a}) = \varphi_2(\varphi_1(\mathbf{a}))$ on some anyon \mathbf{a} . The “separation” between two automorphisms φ_A, φ_B is quantified by the transition map

$$\tau_{BA} = \varphi_B\varphi_A^{-1}. \quad (4)$$

It links φ_B and φ_A by $\varphi_B = \tau_{BA}\varphi_A$ and satisfies $\tau_{AB} = \tau_{BA}^{-1}$. $\text{Aut}[CC]$ can be partitioned by cycle type into 9 conjugacy classes (sets that are linked by conjugation with some element in $\text{Aut}[CC]$), which are subsets of the conjugacy classes of S_6 . For example, $(rg)(xyz)$ and $(rgb)(xy)$ both contain one 2-cycle³ and one 3-cycle and thus both have cycle type $[2^13^1]$. We denote their conjugacy class $\mathcal{C}\{(ccc)(\sigma\sigma)\}$. All 9 conjugacy classes are listed in Table I. τ_{BA} and τ_{AB} are in the same conjugacy class because permutations and their inverses are always of the same cycle type.

A. Anyon Condensation

Anyon condensation is the process of relating two topologically-ordered systems by identifying a set of condensed bosons in the “parent” TO with the vacuum particle in the “child” TO [24, 62–67]; the process has similarities to its namesake Bose-condensations in other physical systems [64]. Crucially, condensing a nontrivial boson, $c\sigma$, in a CC parent phase realizes a child theory equivalent to the toric code TO, denoted as $TC(c\sigma)$ [24]. By condensing different bosons at different times, a system transitions between different child theories. Indeed, the honeycomb Floquet code is equivalent to a dynamical transition through the TOs of $TC(\mathbf{rx}) \rightarrow TC(\mathbf{gy}) \rightarrow TC(\mathbf{bz}) \rightarrow TC(\mathbf{rx}) \rightarrow \dots$ [16]. We diagrammatically represent this sequence using the magic square notation of Eq. (2),



such that the \bullet indicates the condensed boson.

¹ The toric code is characterized by four species of anyons: the vacuum $\mathbf{1}$, bosons \mathbf{e} and \mathbf{m} , and fermion \mathbf{f} . There are 4^2 anyon species in CC and 4 in TC .

² The S_2 subgroup is not closed under conjugation, and hence we require the semidirect product.

³ A k -cycle is a cycle with k labels. It equivalently has order k : if ϕ is a k -cycle then $k \geq 1$ is minimal such that $\phi^k = \text{id}$.

Table I. Conjugacy classes of the automorphism group, $\text{Aut}[CC]$ (see Appendix B). Cycle type states the number of k -cycles that form the automorphisms, with $[3^2]$ indicating two 3-cycles, for example. \mathcal{D}^2 is the square of the quantum dimension of a twist, equal to the number of anyon species that localize at that twist (see Section III). IMS indicates the number of invariant anyons that form mutual-semion pairs \mathbf{a} and \mathbf{b} , such that $\varphi(\mathbf{a}) = \mathbf{a}$, $\varphi(\mathbf{b}) = \mathbf{b}$, with \mathbf{a} and \mathbf{b} having -1 -mutual statistics, and trivial statistics with all other pairs.

Conjugacy Class	Cycle Type	Example	Parity on $S_3 \times S_3$	$\log_2 \mathcal{D}^2$	IMS	Number of Elements
$\mathcal{C}\{\text{id}\}$	$[1^6]$	id	even	0	4	1
$\mathcal{C}\{(\text{c}\sigma)(\text{c}\sigma)(\text{c}\sigma)\}$	$[2^3]$	$(rx)(gy)(bz)$	even	1	2	6
$\mathcal{C}\{(ccc)(\sigma\sigma\sigma)\}$	$[3^2]$	$(rgb)(xyz)$	even	2	2	4
$\mathcal{C}\{(cc)(\sigma\sigma)\}$	$[1^2 2^2]$	$(rg)(xy)$	even	2	0	9
$\mathcal{C}\{(\text{c}\sigma\text{c}\sigma\text{c}\sigma)\}$	$[6^1]$	$(rxgybz)$	even	3	0	12
$\mathcal{C}\{(ccc)\}$	$[1^3 3^1]$	(rgb)	even	4	0	4
$\mathcal{C}\{(cc)\}$	$[1^4 2^1]$	(rg)	odd	2	0	6
$\mathcal{C}\{(\text{c}\sigma\text{c}\sigma)(\text{c}\sigma)\}$	$[2^1 4^2]$	$(rxgy)(bz)$	odd	3	0	18
$\mathcal{C}\{(ccc)(\sigma\sigma)\}$	$[1^1 2^1 3^1]$	$(rgb)(xy)$	odd	4	0	12
Total						72

Importantly, two child theories $TC(\text{c}\sigma_1)$ and $TC(\text{c}\sigma_2)$ are compatible if and only if $\text{c}\sigma_1$ and $\text{c}\sigma_2$ are mutual-semions [26, 32, 78]. This ensures that two regions of $TC(\text{c}\sigma_1)$ and $TC(\text{c}\sigma_2)$ in spacetime share an invertible domain wall: if we start with $TC(\text{c}\sigma_1)$ and condense the $\text{c}\sigma_2$ boson, the quantum state of the TO is preserved. Any anyon in $TC(\text{c}\sigma_1)$ can move across the domain wall and be mapped onto another anyon in $TC(\text{c}\sigma_2)$ without modifying information about the particle (such as its statistics with other anyons). This process of pairing up consecutive compatible child theories $TC(\text{c}\sigma_1) \rightarrow TC(\text{c}\sigma_2)$ is called a “reversible transition”. In the magic square notation, reversible transitions require that consecutive stages condense bosons that share neither the same row nor the same column.

It is also possible to construct a TO where anyon condensation results in a child CC theory. One such example is the “dynamic automorphism” (DA) color code from Ref. 26, using a parent $CC \boxtimes CC$ theory of two color code models; this can be envisaged as the honeycomb lattice with two qubits at each lattice site (or equivalently, two layers of honeycomb lattices) each hosting an independent CC phase. The Hamiltonian is equivalent to Eq. (1), except there are now two of each P_X and P_Z that act only on the first or second layers. Condensing the anyons $\text{r}\mathbf{z}_1\text{r}\mathbf{z}_2$, $\text{g}\mathbf{z}_1\text{g}\mathbf{z}_2$, and thus $\text{b}\mathbf{z}_1\text{b}\mathbf{z}_2$ (where the subscripts indicate the layer) produces a child theory \widetilde{CC} equivalent to the color code.⁴ The anyons of this theory have representatives

$$\begin{array}{ccc|ccc} \text{r}\mathbf{x}_1\text{r}\mathbf{x}_2 & \text{r}\mathbf{y}_1\text{r}\mathbf{x}_2 & \text{r}\mathbf{z}_1 & \text{r}\mathbf{y}_1\text{r}\mathbf{y}_2 & \text{r}\mathbf{x}_1\text{r}\mathbf{y}_2 & \text{r}\mathbf{z}_2 \\ \text{g}\mathbf{x}_1\text{g}\mathbf{x}_2 & \text{g}\mathbf{y}_1\text{g}\mathbf{x}_2 & \text{g}\mathbf{z}_1 & \text{g}\mathbf{y}_1\text{g}\mathbf{y}_2 & \text{g}\mathbf{x}_1\text{g}\mathbf{y}_2 & \text{g}\mathbf{z}_2 \\ \text{b}\mathbf{x}_1\text{b}\mathbf{x}_2 & \text{b}\mathbf{y}_1\text{b}\mathbf{x}_2 & \text{b}\mathbf{z}_1 & \text{b}\mathbf{y}_1\text{b}\mathbf{y}_2 & \text{b}\mathbf{x}_1\text{b}\mathbf{y}_2 & \text{b}\mathbf{z}_2 \end{array} \sim \quad (5)$$

in correspondence to the CC anyons of Eq. (2), with \sim indicating equivalence up to fusion with the condensed

bosons. For example, $\text{r}\mathbf{x}_1\text{r}\mathbf{x}_2 \times \text{r}\mathbf{z}_1\text{r}\mathbf{z}_2 = \text{r}\mathbf{y}_1\text{r}\mathbf{y}_2$. When referring to anyons of \widetilde{CC} , if the subscripts are omitted then we are denoting them by their equivalent sectors in CC ; that is, $\text{r}\mathbf{x}$ refers to $\text{r}\mathbf{x}_1\text{r}\mathbf{x}_2$ or $\text{r}\mathbf{y}_1\text{r}\mathbf{y}_2$.

Condensing an individual anyon from each CC layer alternatively creates a child theory of two decoupled toric codes, denoted $TC(\text{c}\sigma_1) \boxtimes TC(\text{c}\sigma_2)$ with \boxtimes again indicating the tensor product. Reversible transitions now occur in two ways: (1) $TC \boxtimes TC \leftrightarrow TC \boxtimes TC$ are reversible iff the individual TC_1 and TC_2 transitions are reversible; and (2) $\widetilde{CC} \leftrightarrow TC \boxtimes TC$ are reversible iff the two condensed anyons of the $TC \boxtimes TC$ are of different colors and neither are z -flavored⁵ [26].

Crucially, Davydova et al. [26] showed how reversible dynamical sequences starting and ending at \widetilde{CC} can transition the TO in such a way that upon returning to \widetilde{CC} an automorphism is enacted on the anyons. For example, this is a sequence that enacts an (rgb) automorphism,

$$\widetilde{CC} \rightarrow \begin{array}{|c|c|c|} \hline 1 & & \\ \hline & & \\ \hline 2 & & \\ \hline \end{array} \rightarrow \begin{array}{|c|c|c|} \hline & & \\ \hline & & 2 \\ \hline & & 1 \\ \hline \end{array} \rightarrow \begin{array}{|c|c|c|} \hline 2 & & \\ \hline 1 & & \\ \hline & & \\ \hline \end{array} \rightarrow \widetilde{CC} \quad (6)$$

where the 1, 2 labels indicate the condensed boson in the two CC layers, using the magic square notation from Eq. (2). That is, this sequence of anyon condensation maps between the TOs of $\widetilde{CC} \rightarrow TC(\text{r}\mathbf{x}_1) \boxtimes TC(\text{b}\mathbf{x}_2) \rightarrow TC(\text{b}\mathbf{z}_1) \boxtimes TC(\text{g}\mathbf{z}_2) \rightarrow TC(\text{g}\mathbf{y}_1) \boxtimes TC(\text{r}\mathbf{y}_2) \rightarrow \widetilde{CC}$. It is possible to produce all 72 $\text{Aut}[CC]$ -automorphisms of the color code in this way using at most 4 intermediary $TC \boxtimes TC$ condensations [26]; Appendix D explains how to compute the automorphism from any given sequence, or construct a sequence to realize any given automorphism. By repeatedly cycling through a sequence of condensates such as Eq. (6) similarly to a driven quantum

⁴ This is only one such condensation choice; we could condense z -flavored bosons, for example, and achieve an equivalent theory.

⁵ This condition arises due to the choice of z -flavored condensations leading to the child theory \widetilde{CC} .

system, we thus create an evolving phase that exhibits time-periodic, Floquet-enriched topological order (FET) [39]. Anyons present will periodically have their labels permuted. Multiple measurement sequences can realize the same automorphism each Floquet period, and therefore multiple different systems can exhibit the same FET.

B. Dynamical Codes

We may also interpret these FETs as dynamical QEC codes capable of encoding and storing quantum information. We use here the stabilizer formalism [2, 7, 12, 79]: taking the P_X and P_Z plaquette Hamiltonian terms from Eq. (1), we promote them to generators of an Abelian “stabilizer” group \mathcal{S} .⁶ The simultaneous +1-eigenspace of \mathcal{S} defines the codespace C such that $\forall S \in \mathcal{S}$ and $|\psi\rangle \in C$ we have $S|\psi\rangle = |\psi\rangle$. C coincides with the ground space of our Hamiltonian. Excited states $|\psi'\rangle$, for which $S|\psi'\rangle = -|\psi'\rangle$ for some $S \in \mathcal{S}$, are not in the codespace; the “excited” stabilizers indicate that the system has suffered an error. These excited plaquettes are equivalent to the locations of anyon excitations in the Hamiltonian picture. Logical operators map between states within the degenerate codespace C ; these are denoted as \bar{X}, \bar{Z} and act with the same algebra on the (logical) Hilbert space of C as X, Z act on single qubits. All logical operators commute with every stabilizer in \mathcal{S} , forming the centralizer group $C(\mathcal{S})$; the nontrivial logicals are those in the centralizer but not the stabilizer group itself, forming the set $\mathcal{L} = C(\mathcal{S}) \setminus \mathcal{S}$.

To perform anyon condensation, we use projective measurements of the hopping operators for the condensed boson; these are (typically) weight-2 Pauli operators that correspond to moving an excitation through the lattice [24]. For a rx in the color code, for example, it is the 2-qubit X operator on the ends of a red link. Measuring these throughout a system in the codespace of CC causes a $CC \rightarrow TC(rx)$ transition [24]. In doing so, the stabilizer group updates as measured operators are added and anticommuting operators are combined or removed; since this group is constantly changing in a dynamical code, we refer to the current state as the instantaneous stabilizer group (ISG) [16]. The ISG updates during each condensation stage.

In our work, we focus on the $CC \boxtimes CC$ model of the DA color code. In this context, the external tensor product denotes that the stabilizer group of $CC \boxtimes CC$ can be factored (up to a unitary transformation) into two independent copies of CC stabilizer groups [26]. The initial stabilizer group is thus comprised of P_X and P_Z plaquettes on both layers of honeycomb lattices. Forming

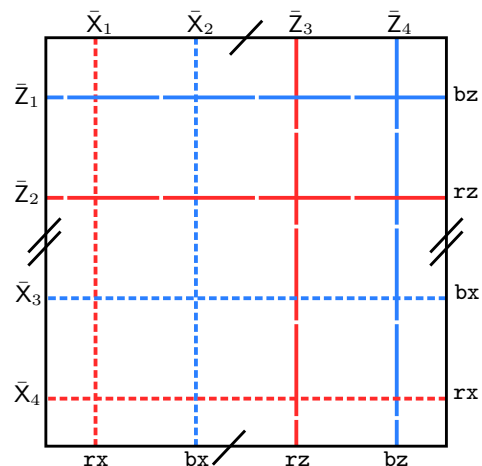


Figure 3. Diagram of the logical operators of the CC model on a 2-torus. Shown are the 4 pairs of anticommuting \bar{X} (short-dashed) and \bar{Z} (long-dashed) operators from Eq. (7)-(10), supported on noncontractible cycles of the 2-torus. The honeycomb lattice structure is ignored for simplicity; the string operators follow the red and blue links of Fig. 2.

the child theory \widetilde{CC} requires projective measurements of $Z_1 Z_2$ on each lattice site, where the subscripts indicate the two layers. $TC \boxtimes TC$ child theories are analogous to the previous discussions, with hopping operators measured on each layer separately for the respective condensed anyons.

Our implementation of the DA color code focuses on a 2-torus that is characterized by linear system size L , such that there are L plaquettes in each of the horizontal and vertical directions,⁷ and joined by periodic boundary conditions on all sides. Future work may find it fruitful to consider other topologies or open boundary conditions. We employ a logical algebra with 4 pairs of anticommuting logical operators constructed out of rx , bz , bx , and rz effective anyon strings. Two operators are equivalent (act equivalently on the ground state) if they are related modulo multiplication with operators in the stabilizer group [2]. This means that multiple representatives of each logical operator exist; on the 2-torus these are supported on homologous noncontractible cycles around the periodic boundaries.⁸ Let $\bar{O}[\mathbf{a}]_h$ and $\bar{O}[\mathbf{a}]_v$ represent the equivalence class of logical operators, forming the quotient group $C(\mathcal{S})/\mathcal{S}$. The subscript indicates that the string wraps around the horizontal or vertical direction respectively (using the orientation of Fig. 2). An italicized $\bar{O}[\mathbf{a}]_h$ indicates a particular representative of the

⁶ A stabilizer group is specifically any subgroup of the n -qubit Pauli group that does not contain -1 and where all the elements commute. It “stabilizes” a code in the sense that any element of the stabilizer group acts trivially on the logical subspace.

⁷ Equivalently, $2L$ lattice sites in the horizontal direction and L lattice sites vertically.

⁸ Two cycles are homologous if one can be smoothly deformed into the other without breaking the chain. A cycle is noncontractible if it is not homologous to a loop with zero area, i.e. a point.

equivalence class. We use the logical algebra

$$\bar{X}_1 = \bar{O}[\mathbf{rx}]_v, \quad \bar{Z}_1 = \bar{O}[\mathbf{bz}]_h, \quad (7)$$

$$\bar{X}_2 = \bar{O}[\mathbf{bx}]_v, \quad \bar{Z}_2 = \bar{O}[\mathbf{rz}]_h, \quad (8)$$

$$\bar{X}_3 = \bar{O}[\mathbf{bx}]_h, \quad \bar{Z}_3 = \bar{O}[\mathbf{rz}]_v, \quad (9)$$

$$\bar{X}_4 = \bar{O}[\mathbf{rx}]_h, \quad \bar{Z}_4 = \bar{O}[\mathbf{bz}]_v. \quad (10)$$

Figure 3 shows sketches of these operators. An automorphism that permutes the anyons now also permutes the logical operators. (rb) , for example, swaps \bar{X}_1 and \bar{X}_2 . Computing the remaining transformations we find that (rb) is equivalent to a $\text{SWAP}_{12}\text{SWAP}_{34}$ gate. All 72 automorphisms furnish a subgroup of the 4-qubit Clifford group [26]. This choice of logical algebra is not unique. Indeed, we are also not restricted to just using bosons; any choice of 4 anyons that form two pairs of mutual-semions but otherwise have trivial mutual statistics (hence commuting string operators) can form a valid logical algebra. Section IV C, for example, describes an alternative logical algebra using fermions.

III. COMPETING AUTOMORPHISMS

In an FET, an automorphism can be visualized as a temporal domain wall periodically overlaying the lattice in spacetime, with anyon worldlines that pass through the domain wall undergoing that automorphism [24]. In this section we introduce a disordered system wherein each period there instead are multiple domain walls that partition the manifold and enact different automorphisms on different subregions. We describe the effects of these “competing automorphisms” on general Abelian TOs and use CC as an example. In Section IV we present a specific microscopic disorder model for the DA color code that realizes this behavior.

We analyze competing automorphisms by considering the effect of two species of domain walls on the ground state of an Abelian TO on the 2-torus. Our considerations readily generalize to more species and other topologies with different genera. We describe the ground state of these systems using the stabilizer formalism. Specifically, let \mathcal{S} be the stabilizer group for the TO and \mathcal{L} the nontrivial logical operators. For CC , \mathcal{L} includes Eqs. (7)-(10) and their representatives. We start from a ground state at $t = 0$ with instantaneous stabilizers $\mathcal{S}_0 = \mathcal{S}$ and logicals $\mathcal{L}_0 = \mathcal{L}$. Before time-step $t = 1$ we partition the manifold and label each contiguous region A or B . To each we simultaneously apply one of two species of temporal domain walls, with automorphisms φ_A and φ_B respectively (one of which may be trivial, and we assume $\varphi_A \neq \varphi_B$), cf. Fig. 4. We may equivalently view this as φ_A being applied everywhere and B -subregions of the lattice chosen to additionally enact τ_{BA} .

There are two main effects that determine the evolution of the system to $t = 1$: firstly, stabilizers in \mathcal{S}_0 may map onto logicals in \mathcal{L} , such that the ISG, i.e., the image \mathcal{S}_1 at $t = 1$ of \mathcal{S}_0 under the enacted automorphisms, may

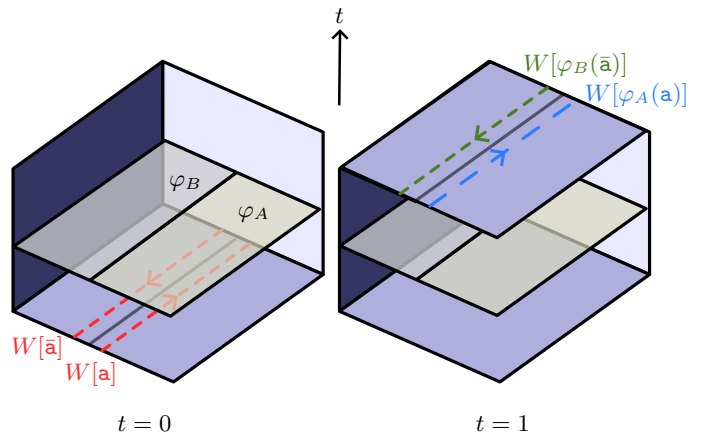


Figure 4. Spacetime illustration of a section of an Abelian TO with time flowing upwards, where φ_A and φ_B domain walls act concurrently on disjoint regions of the lattice between times $t = 0$ and $t = 1$. At $t = 0$, the product of the two operators $W[\mathbf{a}]$ and $W[\bar{\mathbf{a}}]$ with support straddling a (closed) segment of the φ_A - φ_B boundary is trivial and in the stabilizer group. At $t = 1$, this operators evolves to the (potentially nontrivial) product $W[\varphi_A(\mathbf{a})]W[\varphi_B(\bar{\mathbf{a}})]$.

include nontrivial logical operators of the TO, $\mathcal{L} \cap \mathcal{S}_1 \neq \emptyset$. In this case, at least one qubit of logical information has left the logical subspace, and become available to be read out by stabilizer measurements.⁹ Secondly, the logical operators may transform under these automorphisms.

We now examine the first effect. Consider a closed segment of the boundary between φ_A and φ_B domain walls. Let $W[\mathbf{a}]$ denote a string operator for anyon \mathbf{a} along this segment. The operator $O_0 = W[\mathbf{a}]W[\bar{\mathbf{a}}]$ straddling the boundary as in Fig. 4 is a stabilizer at $t = 0$, since $\mathbf{a} \times \bar{\mathbf{a}} = 1$. At $t = 1$, this has evolved to

$$O_1 = W[\varphi_A(\mathbf{a})]W[\varphi_B(\bar{\mathbf{a}})]. \quad (11)$$

Let $\mathbf{b} = \varphi_A(\mathbf{a})$. Then, if $\varphi_A(\mathbf{a}) = \varphi_B(\mathbf{a})$ we have that $\mathbf{b} = \tau_{BA}(\mathbf{b})$. In such a case,

$$\varphi_B(\bar{\mathbf{a}}) = \tau_{BA}(\bar{\mathbf{b}}) = \overline{\tau_{BA}(\mathbf{b})} = \bar{\mathbf{b}}, \quad (12)$$

and so O_1 is still a stabilizer in \mathcal{S} :

$$O_1 = W[\mathbf{b}]W[\bar{\mathbf{b}}] = W[\mathbf{b} \times \bar{\mathbf{b}}] \equiv 1, \quad (13)$$

where the equalities are up to stabilizer products. However, if $\mathbf{b} \neq \tau_{BA}(\mathbf{b})$, then we get

$$O_1 = W[\mathbf{c}], \quad \text{where } \mathbf{c} = \mathbf{b} \times \tau_{BA}(\bar{\mathbf{b}}) \neq 1. \quad (14)$$

⁹ In this analysis, for ease of presentation, we imagine automorphisms and stabilizer measurements occurring at different times. In dynamical code implementations these two processes typically occur simultaneously, hence the logicals in $\mathcal{L} \cap \mathcal{S}_1$ are measured.

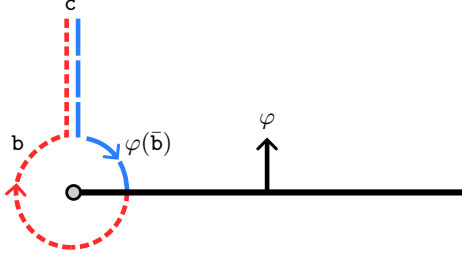


Figure 5. An anyon c decomposes into two anyons \mathbf{b} and $\varphi(\bar{\mathbf{b}})$ in the vicinity of the endpoint (twist) of a domain wall. Moving anticlockwise around the endpoint enacts the automorphism φ . Since $\mathbf{b} \times (\varphi^{-1}\varphi)(\bar{\mathbf{b}}) = 1$, we say that c localizes at the φ twist. This picture applies to both temporal and spatial domain walls, and hence a time arrow is not indicated.

If the segment of the φ_A - φ_B boundary that W follows is a noncontractible cycle of the 2-torus, then O_1 is a logical operator $\bar{O}[c] \in \mathcal{L}$.¹⁰ This $\bar{O}[c]$ evolved from a stabilizer; hence, a logical qubit is now in the +1-eigenspace of this logical operator. The reverse of Fig. 4 also applies: a logical operator at $t = 0$ evolves to a stabilizer at $t = 1$, and logical information encoded at $t = 0$ thus leaves the logical subspace to be detected during stabilizer measurement. These two behaviors jointly enact a logical measurement on the system.

A useful characterization for anyons is localization at domain wall endpoints (or “twists” [80]): if anyon c has fusion channel $c = \mathbf{b} \times \varphi(\bar{\mathbf{b}})$, where φ is the domain wall automorphism for an anyon encircling a twist anticlockwise, it is said to localize at that twist by the process in Fig. 5 [70]. At a φ_A - φ_B boundary, anyon localization of c occurs if $c = \mathbf{b} \times (\varphi_B\varphi_A^{-1})(\bar{\mathbf{b}})$ (cf. Fig. 6). Hence, the anyon c in Eq. (14) localizes at $\tau_{BA} = \varphi_B\varphi_A^{-1}$ twists.

The number of anyons that can localize at a twist equals \mathcal{D}^2 , the square of the quantum dimension \mathcal{D} of the twist. \mathcal{D} tracks the increase in dimension of the Hilbert space when twists are introduced.¹¹ For a \mathbb{Z}_2 TO like CC with each anyon its own antiparticle, $\log_2 \mathcal{D}^2$ indicates the number of independent (under fusion) nontrivial anyon strings introduced to the ISG at a φ_A - φ_B boundary segment; when at least one segment is noncontractible, $\log_2 \mathcal{D}^2$ is also the number of logical qubits measured. If c localizes at τ_{BA} , then for any automorphism φ , $\varphi(c)$ localizes at $\varphi\tau_{BA}\varphi^{-1}$. Hence, the quantum dimension of an automorphism’s twist is a characteristic of its conjugacy class. Table I lists $\log_2 \mathcal{D}^2$ for each conjugacy class in $\text{Aut}[CC]$. Notably, $\mathcal{C}\{(c\sigma)(c\sigma)(c\sigma)\}$ is the

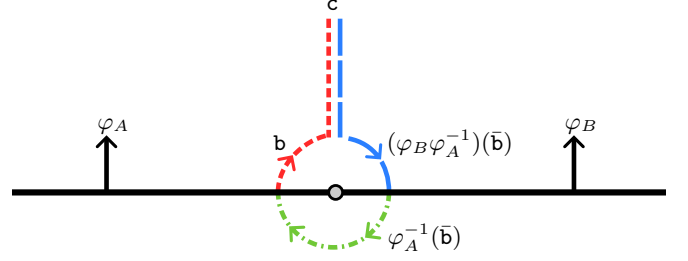


Figure 6. A φ_A and a φ_B domain wall separated by a boundary (indicated by the point). A c anyon that has fusion rule $c = \mathbf{b} \times (\varphi_B\varphi_A^{-1})(\bar{\mathbf{b}})$ localizes at this boundary.

only conjugacy class that measures exactly one logical qubit, $\log_2 \mathcal{D}^2 = 1$; the one nontrivial localized anyon for an automorphism $(c_1\sigma_1)(c_2\sigma_2)(c_3\sigma_3)$ is the fermion $c_1\sigma_1 \times c_2\sigma_2 \times c_3\sigma_3$.

We now consider the second effect: the transformation of logical operators. Representatives of logical operators that have support entirely contained within a φ temporal domain wall transform as

$$\bar{O}[\mathbf{a}] \mapsto \bar{O}[\varphi(\mathbf{a})]. \quad (15)$$

If the domain wall can contain the support of at least one representative of each logical operator, then it cannot have noncontractible boundary segments and hence $\mathcal{L} \cap \mathcal{S}_1 = \emptyset$; no logical operator is measured and \mathcal{L} is preserved. If the φ_A - φ_B boundary has noncontractible segments, then some logical operators will have all representatives intersecting this boundary, cf. Fig. 7. However, Eq. (15) still applies (with $\varphi = \varphi_A$ or φ_B) if $\varphi_A(\mathbf{a}) = \varphi_B(\mathbf{a})$. Equivalently, $\mathbf{b} = \tau_{BA}(\mathbf{b})$ for $\mathbf{b} = \varphi_A(\mathbf{a})$, i.e., \mathbf{b} is invariant under τ_{BA} . Whether this condition holds is set by anyon localization, according to the lemma (proven in Appendix C):

Lemma 1. *For an automorphism τ and anyon \mathbf{b} , $\mathbf{b} = \tau(\mathbf{b})$ if and only if \mathbf{b} and c braid trivially for all anyons c that localize at τ .*

An important consequence of this lemma is that if \mathbf{b}_1 and \mathbf{b}_2 are mutual-semions that are both invariant under τ_{BA} , then neither \mathbf{b}_1 nor \mathbf{b}_2 can localize at τ_{BA} . The logical operators $\bar{O}[\mathbf{a}_1]_v$ and $\bar{O}[\mathbf{a}_2]_h$ [with $\mathbf{b}_1 = \varphi_A(\mathbf{a}_1)$, $\mathbf{b}_2 = \varphi_A(\mathbf{a}_2)$] anticommute, forming a logical \bar{X} and \bar{Z} that satisfy Eq. (15). Moreover, they do not map onto one of the measured $W[c]$ φ_A - φ_B boundary-operators, and they also commute with all such measurements. The existence of an invariant mutual-semion pair under τ_{BA} thus guarantees a logical qubit that is not measured in any partition of competing φ_A and φ_B domain walls. We call this a “protected” logical qubit. Since both $(\bar{O}[\mathbf{a}_1]_v, \bar{O}[\mathbf{a}_2]_h)$ and $(\bar{O}[\mathbf{a}_1]_h, \bar{O}[\mathbf{a}_2]_v)$ form anticommuting \bar{X} and \bar{Z} pairs, we in fact have two protected qubits per invariant mutual-semion pair. If an anyon \mathbf{b} is invariant under τ_{BA} , then for any automorphism φ , $\varphi(\mathbf{b})$ is invariant under the conjugate automor-

¹⁰ Distinct noncontractible segments of a boundary around homologous cycles create $\bar{O}[c]$ that are representations of equivalent logical operators, because the boundary as a whole is homologically trivial.

¹¹ This relation applies only for Abelian anyon theories; in non-Abelian theories, one must also consider the quantum dimension of localizing anyons [31, 70, 81].

phism $\varphi_{\tau_{BA}}\varphi^{-1}$. Hence, the number of invariant mutual-semion pairs characterizes the conjugacy class of τ_{BA} . For $\tau_{BA} \in \text{Aut}[CC]$, the only conjugacy classes with such pairs are $\mathcal{C}\{\text{id}\}$, $\mathcal{C}\{(\sigma\sigma)(\sigma\sigma)(\sigma\sigma)\}$ and $\mathcal{C}\{(ccc)(\sigma\sigma\sigma)\}$, cf. Table I. For example, $\tau_{BA} = (rx)(gy)(bz)$ has rx and bz as invariant mutual-semions.

These two properties—localized and invariant anyons—set the extent to which a completely mixed logical state purifies over one period of competing automorphisms. $\log_2 \mathcal{D}^2$ indicates the number of logical qubits measured if the boundaries of the competing automorphisms contain noncontractible segments. The number of invariant mutual-semions (IMS) is the number of such logical qubits that will not be measured out, regardless of the particular domain wall configurations. For example, if $\log_2 \mathcal{D}^2 = 2$ and $\text{IMS} = 0$ for the CC model on the 2-torus, then although 2 of the 4 qubits will not be measured out between $t = 0$ and $t = 1$ in any given domain wall configuration, the measured 2 qubits for $W[c]$ of Eq. (14) along each of the noncontractible cycles span the logical space.¹² On the other hand, $\text{IMS} = 2$ means that the same 2 logical qubits are protected in any configuration.

What about multiple consecutive realizations of competing automorphisms? Consider that between $t = 1$ and $t = 2$ we again (randomly) partition the manifold and enact φ_A and φ_B . Assume that the φ_A - φ_B boundaries contain noncontractible segments such that logical operators are measured. If a protected logical qubit exists from $t = 0$ to $t = 2$, there must be mutual-semions that braid trivially with the anyons c that localize at τ_{BA} between $t = 0$ and $t = 1$. They must also braid trivially with the anyons that will localize between $t = 1$ and $t = 2$, that is $\varphi_A^{-1}(c)$ or $\varphi_B^{-1}(c)$. If all localized anyons braid trivially (in the CC model, this is guaranteed whenever there is a single nontrivial localized anyon, $\log_2 \mathcal{D}^2 = 1$), then Lemma 1 tells us that $\varphi_A^{-1}(c) = \varphi_B^{-1}(c)$. Extending this argument to $t \rightarrow \infty$, we therefore have two protected logical qubits for each pair of mutual-semions that braid trivially with $\varphi_A^{-t}(c)$ for $t = 0, 1, 2, \dots$ and for all c that localize at τ_{BA} . If not all localized anyons have trivial mutual statistics,¹³ then requiring that the mutual-semions braid trivially with all $(\varphi_t\varphi_{t-1}\dots\varphi_1)(c)$ where each $\varphi_i \in \{\varphi_A^{-1}, \varphi_B^{-1}\}$ and $t = 0, 1, 2, \dots$ is a sufficient condition for a protected logical qubit.

We now summarize the main effects of different partitions of competing automorphisms. We call a configuration of φ_A and φ_B temporal domain walls φ_A -dominant if the A -labelled subregions can completely contain a noncontractible cycle from every homology class. That is,

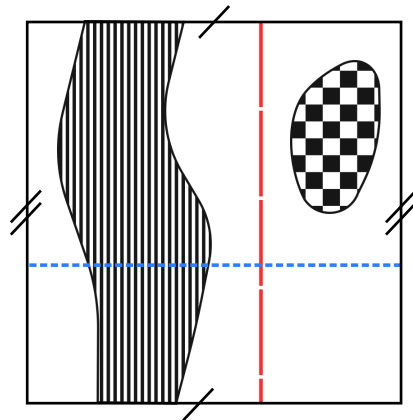


Figure 7. A 2-torus showing two temporal domain walls. If the boundary of a domain wall has only contractible segments (checked region), there exists at least one representative of each logical operator (red and blue lines) that avoids intersecting the boundary. On the other hand, a domain wall with a noncontractible boundary segment (striped region) always bisects one of each \bar{X} , \bar{Z} logical operator pairs.

the support of a representation of each logical operator can be contained within the A -subregions. φ_B -dominant configurations are defined analogously. Eq. (15)—with $\varphi = \varphi_A$ or φ_B respectively—holds for a representative of each logical operator. In these configurations, the φ_A - φ_B boundaries have only contractible segments. \mathcal{L} can be preserved; logical information is not necessarily lost or measured. However, if the φ_A - φ_B boundaries contain noncontractible segments, such as the striped region in Fig. 7,¹⁴ then at least one logical operator is measured corresponding to the nontrivial anyons that localize at τ_{BA} . A necessary condition for any logical qubit to be protected over one period of any random realization is that it must have its \bar{X} and \bar{Z} formed from mutual-semions that satisfy $\varphi_A(\mathbf{a}) = \varphi_B(\mathbf{a})$, or equivalently $\mathbf{b} = \tau_{BA}(\mathbf{b})$ for $\mathbf{b} = \varphi_A(\mathbf{a})$ (i.e., \mathbf{b} is invariant under τ_{BA}). The number of invariant or localized anyons is characteristic of each τ_{BA} 's conjugacy class.

IV. DA DISORDER MODEL

To illustrate the usefulness of these results and the competing automorphism picture, we now present a specific microscopic disorder model, based on the DA color code [26], that realizes these systems for CC . In Section II, we constructed measurement sequences that can

¹² This occurs when the localized anyons braid trivially with each other.

¹³ In the CC model nontrivial mutual statistics is required for $\log_2 \mathcal{D}^2 > 1$ with $\text{IMS} > 0$, otherwise four commuting logicals can be measured on conjugate noncontractible φ_A - φ_B boundary cycles.

¹⁴ In addition to the example striped region in Fig. 7, the boundary might alternatively contain a noncontractible segment extending around both cycles of the torus. In this case, the measured logical operator is equivalent to a product of \bar{O}_v and \bar{O}_h logical operators using the algebra in Fig. 3. The resulting behavior is therefore analogous to the case discussed here.

A. Adjacent FETs

In this section, we examine the properties of the disorder model in more detail. In particular, what pairs of FETs can compete? We introduce the definition:

Definition 1 (Adjacent FETs). *Two FETs A and B with automorphisms φ_A and φ_B are adjacent if there exists a 1-component disorder model that realizes competing φ_A and φ_B temporal domain walls.*

At criticality, a 1-component disorder model measures exactly one logical qubit (with high probability); by Section III, this necessitates that τ_{BA} has $\log_2 \mathcal{D}^2 = 1$. From Table I, for $\text{Aut}[CC]$ there is only one conjugacy class for which this is true. Two FETs in the DA color code are thus adjacent only if their automorphisms satisfy the *separation condition*

$$\tau_{BA} \in \mathcal{C}\{(\epsilon\sigma)(\epsilon\sigma)(\epsilon\sigma)\}. \quad (17)$$

There are several immediate consequences of this:

- (1) The trivial FET, $\mathbb{1}$, with $\varphi = \text{id}$ is adjacent only to FETs with automorphisms in the $\mathcal{C}\{(\epsilon\sigma)(\epsilon\sigma)(\epsilon\sigma)\}$ conjugacy class. This follows from $\varphi_B = \tau_{BA} \cdot \text{id}$.
- (2) Adjacent FETs always have different parities on the S_2 subgroup of $\text{Aut}[CC]$ (color-flavor exchange, c.f. Appendix B 2), but the same parities on the $S_3 \times S_3$ subgroup (color or flavor permutations). This comes from τ_{BA} having odd-parity on the S_2 subgroup, but even-parity on the $S_3 \times S_3$ subgroup.
- (3) Two FETs in the same conjugacy class are never adjacent, since elements of a conjugacy class have the same parities on all subgroups.
- (4) The logical operator that is measured when the system is tuned near the critical point must be a fermion string. This is because there is precisely one nontrivial anyon—a fermion—that localizes at twists corresponding to the automorphisms in $\mathcal{C}\{(\epsilon\sigma)(\epsilon\sigma)(\epsilon\sigma)\}$ [70]. For a $(c_1\sigma_1)(c_2\sigma_2)(c_3\sigma_3)$ automorphism, this fermion is $c_1\sigma_1 \times c_2\sigma_2 \times c_3\sigma_3$.

We can promote this separation condition to a sufficient and necessary condition by showing that for all FET pairs with automorphisms satisfying Eq. (17) there exists a measurement sequence and 1-component disorder model that connects them. We first introduce the idea of concatenating two measurement sequences: let $\mathcal{A}_i, \mathcal{C}_j$ denote some $TC \boxtimes TC$ child theories. For a sequence

$$\widetilde{CC} \rightarrow \mathcal{A}_1 \rightarrow \cdots \rightarrow \mathcal{A}_m \rightarrow \widetilde{CC} \quad (18)$$

that realizes automorphism φ_A , and a sequence

$$\widetilde{CC} \rightarrow \mathcal{A}_m \rightarrow \mathcal{C}_1 \rightarrow \cdots \rightarrow \mathcal{C}_n \rightarrow \widetilde{CC} \quad (19)$$

that realizes automorphism φ_C , we can construct the concatenated sequence

$$\widetilde{CC} \rightarrow \mathcal{A}_1 \rightarrow \cdots \rightarrow \mathcal{A}_m \rightarrow \mathcal{C}_1 \rightarrow \cdots \rightarrow \mathcal{C}_n \rightarrow \widetilde{CC} \quad (20)$$

that realizes automorphism $\varphi_C\varphi_A$. Now, the trivial FET, $\mathbb{1}$, is adjacent to all FETs in $\mathcal{C}\{(\epsilon\sigma)(\epsilon\sigma)(\epsilon\sigma)\}$; we explicitly provide example 1-component disorder models in Appendix E to prove this. Then, let A and B be any two FETs with automorphisms φ_A and φ_B that satisfy the separation condition, $\tau_{BA} \in \mathcal{C}\{(\epsilon\sigma)(\epsilon\sigma)(\epsilon\sigma)\}$. It is possible (see Appendix D) to construct a measurement sequence for A such that its final $TC \boxtimes TC$ child theory is the same as the first $TC \boxtimes TC$ child theory of the measurement sequence that connects id and τ_{BA} via a 1-component disorder model. Using the result above, we concatenate the measurement sequence for A with the measurement sequence that realizes $\varphi_C = \text{id}$ or $\varphi_C = \tau_{BA}$. We now have a 1-component disorder model that creates automorphisms $\varphi_A = \text{id} \cdot \varphi_A$ and $\varphi_B = \tau_{BA}\varphi_A$. Thus, two FETs are adjacent if and only if their automorphisms satisfy Eq. (17).

The space of FETs in which Eq. (17) establishes adjacency labels FETs solely by their automorphisms. Hence in this space, distinct measurement sequences realizing the same automorphism are identified. Eq. (17) is an existence condition for suitable measurement sequences realizing FETs A and B ; it does not guarantee that there is a 1-component disorder model involving any given two measurement sequences realizing FETs A and B .

B. Connected FETs

Competing automorphisms and 1-component disorder models provide a natural method of interpolating between different FETs by modifying one part of their measurement cycle. What additional structure emerges when we consider the space of these adjacent FETs? To answer this, we introduce an extension of adjacency:

Definition 2 (Connected FETs). *Two FETs, A_0 and A_m , are connected if there exists an adjacency sequence of FETs $\{A_0, A_1, \dots, A_m\}$, such that A_i and A_{i+1} are adjacent for all $i = 0, \dots, m-1$. The length of this sequence is defined as m .*

In interpreting this definition, we recall that we work with a space of FETs that identifies distinct measurement sequences realizing the same FET. Hence for each $j = 1, \dots, m-1$, we allow for FET A_j to be realized by distinct measurement sequences in the 1-component disorder models connecting it to A_{j-1} and to A_{j+1} .¹⁵

Based on this definition, we pose the question: are any two arbitrary FETs connected? Equivalently, constructing the graph $G = (N, E)$ with each node in N a distinct FET and an edge in E joining adjacent FETs, is this graph connected? If two nodes $n, m \in N$ are joined

¹⁵ In a space that distinguishes distinct measurement sequences, different measurement sequences realizing the same FET may not be connected in the sense of Definition 2, see App. F.

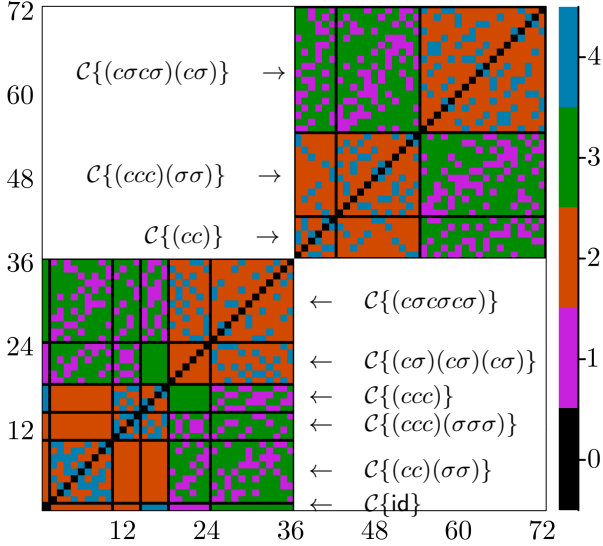


Figure 9. Each row and column corresponds to one of the 72 automorphisms in $\text{Aut}[CC]$, grouped by conjugacy class. The color indicates the minimum number of edges connecting the nodes in G associated with the row and column automorphisms; equivalently, it is the length of the minimum adjacency sequence connecting the two FETs of those automorphisms. There are two distinct clusters, grouped by their parity on the $S_3 \times S_3$ subgroup; even-parity automorphisms are in the bottom left quadrant and odd-parity in the top right quadrant. White squares indicate that there is no possible adjacency sequence to connect those two FETs.

by an edge, then their automorphisms φ_n, φ_m satisfy $\tau_{mn} \in \mathcal{C}\{(\sigma)(\sigma)(\sigma)\}$. By Section IV A, $\varphi_m = \tau_{mn}\varphi_n$ has the same parity on $S_3 \times S_3$ as φ_n . There is thus no path in G connecting two FETs with automorphisms of different parity on $S_3 \times S_3$, and G has (at least) two non-empty connected components. Each component contains 36 FETs, grouped by the conjugacy class of their automorphisms (cf. Table I).¹⁶

We numerically compute all inequivalent 1-component disorder models by enumerating the possible isomorphism contributions (see Appendix D), thus specifying the graph G . Figure 9 shows the minimum graph distances on G between all FETs, as well as displaying the separation into exactly two connected components.

We can explain these distances, starting from the simple case of transitions from the trivial FET: We begin with the sequence of two adjacent FETs $\{\mathbb{1}, A_1\}$. Using a 1-component disorder model, if A_1 is adjacent

to the trivial FET then its automorphism φ_1 satisfies $\varphi_1 = \tau_{10} \cdot \text{id} = \tau_{10}$, where $\tau_{10} \in \mathcal{C}\{(\sigma)(\sigma)(\sigma)\}$. Any automorphism in $\mathcal{C}\{(\sigma)(\sigma)(\sigma)\}$ can be realized from the identity using a 1-component disorder model, as discussed in Section IV A.

Since these automorphisms exchange color and flavor, we can interpret τ_{10} geometrically as a reflection of the magic square (placed on a 2-torus) along a mirror line parallel to the diagonal or antidiagonal. Specifically, the mirror line intersects the three bosons listed by the three 2-cycles of the automorphism. $(ry)(gz)(bx)$, for example, has a mirror line through anyons ry , gz , and bx .

For a sequence $\{\mathbb{1}, A_1, A_2\}$, the associated automorphism for A_2 must satisfy $\varphi_2 = \tau_{21}\varphi_1 = \tau_{21}\tau_{10}$, where both $\tau_{21}, \tau_{10} \in \mathcal{C}\{(\sigma)(\sigma)(\sigma)\}$ are such reflections. If $\tau_{21} = \tau_{10}$ we arrive back at id . Otherwise, there are two scenarios to consider:

- (1) If the two mirror lines are perpendicular, then by the *Compositions of Reflections over Intersecting Lines Theorem*, this enacts a rotation by π about their intersection. This populates the $\mathcal{C}\{(cc)(\sigma\sigma)\}$ conjugacy class. There are 9 such intersections (each entry of the magic square), agreeing with the class's number of elements in Table I.
- (2) If the two mirror lines are parallel, then by the *Reflection in Parallel Lines Theorem*, this enacts a translation normal to the two lines. That is, φ_2 translates along either the diagonal or antidiagonal directions of the magic square, and thus belongs to $\mathcal{C}\{(ccc)(\sigma\sigma\sigma)\}$. There are two directions and two nontrivial and nonequivalent magnitudes of translation, forming the 4 elements in this class.

There are two more conjugacy classes remaining in the even-parity component: $\mathcal{C}\{(cc\sigma\sigma)\}$ and $\mathcal{C}\{(ccc)\}$. We can realize any automorphism in the former class, e.g. $(c_1\sigma_1c_2\sigma_2c_3\sigma_3)$, with a sequence $\{\mathbb{1}, A_1, A_2, A_3\}$ by choosing $\tau_{32} = (c_1\sigma_3)(c_2\sigma_2)(c_3\sigma_3)$ and $\tau_{21}\tau_{10} = (c_1c_3)(\sigma_1\sigma_2)$ such that $\varphi_3 = \tau_{32}\tau_{21}\tau_{10}$. It is not possible to realize $\mathcal{C}\{(ccc)\}$ with such a sequence because this class has trivial S_2 components but an odd number of τ reflections results in a net nontrivial reflection. Rather, using a sequence $\{\mathbb{1}, A_1, A_2, A_3, A_4\}$ we can compose a diagonal translation $\tau_{43}\tau_{32}$ with an antidiagonal translation $\tau_{21}\tau_{10}$ such that $\varphi_4 = \tau_{43}\tau_{32}\tau_{21}\tau_{10}$ translates along the vertical or horizontal directions of the magic square, realizing any $\mathcal{C}\{(ccc)\}$.¹⁷

For any two arbitrary FETs in the same component, A and B , with associated automorphisms φ_A and φ_B ,

¹⁶ There is no direct interpretation of these two components in terms of logical gates. In particular, the mapping from automorphisms to gates is intrinsically dependent on the geometry and boundary conditions of the manifold. For a fixed algebra on the 2-torus, each automorphism can be written as a logical gate in the 4-qubit Clifford group. No apparent structure emerges, however, when viewing these gates grouped by their parity.

¹⁷ We can also show that these are the minimum graph distances between each FET by considering the \mathcal{D}^2 of the conjugacy classes. The reflections $\mathcal{C}\{(\sigma)(\sigma)(\sigma)\}$ have $\mathcal{D}^2 = 2$. $\mathcal{C}\{(ccc)(\sigma\sigma\sigma)\}$ and $\mathcal{C}\{(cc)(\sigma\sigma)\}$ have $\mathcal{D}^2 = 4$, requiring two reflections to populate a fusion group with the required number of localized anyons. Similarly, $\mathcal{C}\{(cc\sigma\sigma)\}$ has $\mathcal{D}^2 = 8$ and $\mathcal{C}\{(ccc)\}$ has $\mathcal{D}^2 = 16$, requiring three and four reflections respectively.

the minimum graph distance between them can be found by identifying the minimum graph distance between the trivial FET and the FET with automorphism τ_{BA} . That is, let the minimum adjacency sequence between $\mathbb{1}$ and the FET with automorphism τ_{BA} be $\{\mathbb{1}, A_1, \dots, A_{\tau_{BA}}\}$ containing $m + 1$ FETs. Then by concatenating each of the m 1-component disorder models in this adjacency sequence with the measurement sequence for A , we get $\{A, A \cdot A_1, \dots, A \cdot A_{\tau_{BA}} = B\}$ (with \cdot used informally here to denote the result of concatenating the two measurement sequences of those FETs). There does not exist a shorter adjacency sequence between A and B , because if there did then we could perform the reverse process and concatenate each of its FETs with a measurement sequence for φ_A^{-1} , thereby realizing an adjacency sequence between $\mathbb{1}$ and τ_{BA} with less than $m + 1$ FETs. For example, take (rb) and $(rgb)(xy)$. Their transition map is $\tau = (rgb)(xy) \cdot (rb)^{-1} = (gb)(xy)$, which is connected to the trivial FET via a graph distance of 2, and thus the FETs with automorphisms (rb) and $(rgb)(xy)$ are also connected via a graph distance of 2.

1-component disorder models therefore prompt a notion of connectivity between FETs of the DA color code. We have seen that two FETs with different parity on the $S_3 \times S_3$ subgroup cannot be connected in this way, and the minimum length adjacency sequence for two FETs with automorphisms φ_A and φ_B is found by taking the minimum length sequence between the trivial FET and the FET with automorphism τ_{BA} .

C. Logically-Connected FETs

We have so far stated sufficient and necessary conditions on the theoretical ability for disorder to generate different automorphisms and FETs. We now consider the behavior of the systems evolving over multiple periods of these measurement sequences, especially away from the deterministic cases of $p = 0$ or 1. In particular, we focus on the effect that disorder has on the logical subspace.

One characteristic quality of this evolution is whether some logical qubits remain protected despite this disorder. In the long-time limit, this number will always be even: if an operator $\bar{O}[c]_v$ is measured, the commuting operator $\bar{O}[c]_h$ can also be measured under a different disorder realization in subsequent periods. A code evolving under a particular disorder model will therefore always have 0, 2, or 4 qubits measured out (or conversely, protected) in the limit of $t \rightarrow \infty$ periods. To quantify which competing automorphisms permit such protected qubits, we introduce a stricter definition of connectedness:

Definition 3 (Logically-Connected). *Two FETs A_0 and A_m are logically-connected if there exists an adjacency sequence of FETs $\{A_0, \dots, A_m\}$ with a consistent non-zero-dimensional logical Hilbert subspace that remains protected in the limit of $t \rightarrow \infty$ periods, for any $p \in [0, 1]$ in any of the m sets of 1-component disorder models between FETs A_i and A_{i+1} .*

Here, “consistent” means that the same logical Hilbert subspace is protected in all of the 1-component disorder models; we interpret this as there being a logical degree of freedom that is unaffected by the disorder modifying A_0 into A_m . By definition, any A_i, A_j in the sequence are also logically-connected, and logically-connected FETs are necessarily also connected FETs.

We first consider adjacent FETs. Let φ_A and φ_B be the two competing automorphisms. The nontrivial anyon that localizes at $\tau_{BA} \in \mathcal{C}\{(c\sigma)(c\sigma)(c\sigma)\}$ is a fermion, which braids trivially with itself and the vacuum. From Section III, if all anyons c that localize at τ_{BA} braid trivially, then each pair of mutual-semions that are invariant under τ_{BA} and braid trivially with all $\varphi_A^{-t}(c)$ for $t = 0, 1, 2, \dots$ guarantees the existence of 2 protected logical qubits as $t \rightarrow \infty$.

This allows us to restrict which automorphisms can be logically-connected; to do so, we first explain how automorphisms map the fermions of the color code. As detailed in Appendix A, there are 6 fermions, forming two fermion groups F and F' with -1 mutual statistics between different fermions within the same group and trivial mutual statistics otherwise. These fermions are mapped by automorphisms according to the lemma:

Lemma 2. *For any fermion \mathbf{f} , if the automorphism φ has even parity on the subgroup $S_3 \times S_3$, then the fermion $\varphi(\mathbf{f})$ is in the same fermion group as \mathbf{f} . If the parity is odd, then $\varphi(\mathbf{f})$ is in the other fermion group.*

A proof of this is provided in Appendix A.

Now, if two fermions are in different fermion groups, there is no fermion that braids trivially with both. Moreover, using the “fermion magic square” from Appendix A, a given fermion $\mathbf{f} \in F$ only braids trivially with the bosons in its row (and the vacuum). For example, $\mathbf{ry} \times \mathbf{bx} \times \mathbf{gz}$ only braids trivially with the \mathbf{ry}, \mathbf{bx} , and \mathbf{gz} bosons. Similarly, $\mathbf{f}' \in F'$ only braids trivially with the bosons in its column. Therefore, the sole boson that braids trivially with both \mathbf{f} and \mathbf{f}' is the boson at the intersection of the row and column. By Lemma 2, for any fermion \mathbf{f} there thus exists one nontrivial anyon, not a pair of mutual-semions, that braids trivially with both \mathbf{f} and $\varphi^{-1}(\mathbf{f})$ if φ has odd-parity on $S_3 \times S_3$ (note that the parity of φ and φ^{-1} are the same). Hence, two FETs with automorphisms with odd-parity on $S_3 \times S_3$ cannot be logically-connected. Moreover, since FETs in the odd-parity component are connected only to other FETs in the odd-parity component, this means that they are logically-connected to no FET. Any 1-component disorder model involving an odd-parity FET and tuned near the critical point will necessarily measure out all 4 logical qubits given enough time.

We now consider FETs connected via a sequence of adjacent FETs $\{A_0, A_1, \dots, A_m\}$ with automorphisms $\varphi_0, \varphi_1, \dots, \varphi_m$. If there exists a common protected logical subspace in the 1-component disorder models between each pair of FETs A_i and A_{i+1} , then the localized fermion in each case must be from the same fermion group. We

Table II. Protected logical algebra for a localized F -fermion.

Operator	Anyon Representation	Equivalent Logical
\tilde{X}_1	$\bar{O}[\mathbf{rx} \times \mathbf{bz}]_v$	$\bar{X}_1 \bar{Z}_4$
\tilde{Z}_1	$\bar{O}[\mathbf{rz} \times \mathbf{by}]_h$	$\bar{Z}_1 \bar{Z}_2 \bar{X}_3$
\tilde{X}_2	$\bar{O}[\mathbf{rx} \times \mathbf{bz}]_h$	$\bar{Z}_1 \bar{X}_4$
\tilde{Z}_2	$\bar{O}[\mathbf{rz} \times \mathbf{by}]_v$	$\bar{X}_2 \bar{Z}_3 \bar{Z}_4$

note the lemma (proof in Appendix A):

Lemma 3. *If two reflections $\tau_1, \tau_2 \in \mathcal{C}\{(\bar{c}\sigma)(\bar{c}\sigma)(\bar{c}\sigma)\}$ are about parallel mirror lines of the magic square, then their localized anyons are fermions in the same fermion group. Otherwise, they are in different fermion groups.*

Therefore, for this condition to hold, each $\tau_{(i+1)i}$ must be a reflection about a mirror line parallel to all other $\tau_{(j+1)j}$ in the adjacency sequence, with $i, j = 0, \dots, m-1$. By the *Reflection in Parallel Lines Theorem*, the only possible conjugacy classes created from an even number of these reflections are translations along a diagonal of the magic square, that is $\mathcal{C}\{\text{id}\}$ or $\mathcal{C}\{(\bar{c}\bar{c}\bar{c})(\sigma\sigma\sigma)\}$. An odd number of reflections results in another reflection about a parallel mirror line. Therefore, assuming that $A_0 \neq A_m$, a necessary condition for A_0 and A_m to be logically-connected is that

$$\tau_{m0} \in \mathcal{C}\{(\bar{c}\bar{c}\bar{c})(\sigma\sigma\sigma)\} \quad (21)$$

for even m , or

$$\tau_{m0} \in \mathcal{C}\{(\bar{c}\sigma)(\bar{c}\sigma)(\bar{c}\sigma)\} \quad (22)$$

for odd m . Furthermore, we know from Section IV B that if $\tau_{BA} \in \mathcal{C}\{(\bar{c}\sigma)(\bar{c}\sigma)(\bar{c}\sigma)\}$ then FETs A and B are adjacent, and if $\tau_{BA} \in \mathcal{C}\{(\bar{c}\bar{c}\bar{c})(\sigma\sigma\sigma)\}$ then FETs A and B are connected using two 1-component disorder models. Moreover, in a valid FET with reversible condensations we conjecture that there is no other mechanism for affecting the logical subspace beyond the measured fermions discussed here, and so these conditions should guarantee the existence of a consistent protected non-zero dimensional logical subspace. Assuming this conjecture to be true, any two arbitrary FETs A and B are logically-connected iff their automorphisms have even parity on $S_3 \times S_3$, and τ_{BA} satisfies either Eq. (21) or Eq. (22).

For models where there is a protected logical subspace, these results also enable a prescription to identify representatives of its protected logical operators: for $S_3 \times S_3$ even-parity automorphisms, $\varphi^{-t}(\mathbf{f})$ are guaranteed to be in the same fermion group for all integers $t \geq 0$ by Lemma 2. Therefore, the protected logical operators are constructed out of fermions from the other group, which are guaranteed to braid trivially with all measured fermions. There are thus two possible candidates for logical subspaces that are protected in a 1-component disorder model: if the localized fermion belongs to the F fermion group, then a representative logical algebra is

Table III. Protected logical algebra for a localized F' -fermion.

Operator	Anyon Representation	Equivalent Logical
\tilde{X}_1	$\bar{O}[\mathbf{rz} \times \mathbf{bx}]_v$	$\bar{X}_2 \bar{Z}_3$
\tilde{Z}_1	$\bar{O}[\mathbf{rx} \times \mathbf{by}]_h$	$\bar{Z}_1 \bar{X}_3 \bar{X}_4$
\tilde{X}_2	$\bar{O}[\mathbf{rz} \times \mathbf{bx}]_h$	$\bar{Z}_2 \bar{X}_3$
\tilde{Z}_2	$\bar{O}[\mathbf{rx} \times \mathbf{by}]_v$	$\bar{X}_1 \bar{X}_2 \bar{Z}_4$

given by Table II; if it belongs to the F' fermion group, then we instead use Table III. Notably, the time-evolution of an observable from this algebra at point $p \in [0, 1]$ in any logically-connected 1-component disorder model is indistinguishable from any other point $\tilde{p} \in [0, 1]$.

D. m -Component Disorder Models

We have so far considered only pairs of FETs that arise from 1-component disorder models; we now generalize our results to m -component disorder models where we introduce m parameters $p_1, \dots, p_m \in [0, 1]$ that determine the probability of independently measuring links in m components of the measurement sequence. For example, a 2-component disorder model with two independent disordered stages and probabilities p_1 and p_2 is

$$\begin{aligned} \widetilde{CC} &\rightarrow \begin{array}{|c|c|c|} \hline 1 & & \\ \hline 2 & & \\ \hline \end{array} \rightarrow \begin{array}{|c|c|c|} \hline & 2 & 1 \\ \hline & & \\ \hline \end{array} \rightarrow \underbrace{\begin{array}{|c|c|c|} \hline & & \\ \hline & & \\ \hline & & 1 \\ \hline \end{array}}_{p_1} \\ &\rightarrow \begin{array}{|c|c|c|} \hline 1 & & \\ \hline 2 & & \\ \hline \end{array} \rightarrow \underbrace{\begin{array}{|c|c|c|} \hline & 2 & \\ \hline & & \\ \hline \end{array}}_{p_2} \rightarrow \widetilde{CC}. \end{aligned} \quad (23)$$

We can associate such a model with a 2-dimensional parameter space $[0, 1]^2$ indexed by vectors $\mathbf{p} = (p_1, p_2)$. The four corners of this parameter space have measurement sequences that enact four different automorphisms:

$$\begin{array}{c|cc} & p_1 & \\ \hline p_2 & & \\ \hline 0 & \text{id} & (rx)(gy)(bz) \\ \hline 1 & (rz)(gx)(by) & (rgb)(xzy) \\ \hline \end{array} \quad (24)$$

Additional examples are given in Appendix E. Within an m -dimensional parameter space we can define a trajectory $\mathbf{p}(p) \in [0, 1]^m$ that interpolates between the FETs at two different corners, with $p \in [0, 1]$ such that $\mathbf{p}(0)$ realizes FET A and $\mathbf{p}(1)$ realizes FET B . For example, in the case above, $\mathbf{p}(p) = (p, p)$ maps between the FETs with automorphism id at $p = 0$ and $(rgb)(xzy)$ at $p = 1$. For these trajectories to map valid FETs, we require that the two measurement sequences associated with these endpoints in parameter space are composed of only reversible pairs of condensations.

This construction, however, does not necessitate that the other corners of the parameter space (or midpoints of the trajectory) are also composed of only reversible pairs of condensations. Indeed, modifying Eq. (16) into a 2-component disorder model by

$$\begin{aligned}
\widetilde{CC} &\rightarrow \begin{array}{|c|c|c|} \hline 1 & & \\ \hline & & \\ \hline 2 & & \\ \hline \end{array} \rightarrow \begin{array}{|c|c|c|} \hline & & \\ \hline & & 2 \\ \hline & & \\ \hline \end{array} \rightarrow \begin{array}{|c|c|c|} \hline & & \\ \hline & & \\ \hline & & 1 \\ \hline \end{array} \\
&\hspace{10em} \underbrace{\hspace{10em}}_{p_1} \\
&\rightarrow \begin{array}{|c|c|c|} \hline & 2 & \\ \hline & & \\ \hline & & \\ \hline \end{array} \rightarrow \begin{array}{|c|c|c|} \hline & & \\ \hline & & 1 \\ \hline & & \\ \hline \end{array} \rightarrow \widetilde{CC} \quad (25) \\
&\hspace{10em} \underbrace{\hspace{10em}}_{p_2}
\end{aligned}$$

shows such a case: at any point with $p_2 = 0$, the mapping $TC(\mathbf{gy}_1) \boxtimes TC(\mathbf{gz}_2) \rightarrow \widetilde{CC}$ is irreversible because of the z label in our \widetilde{CC} condensed anyons (cf. the reversibility conditions in Section II A). We call the parameter regions associated with these irreversible measurement sequences “irreversible phases”. We may still define a trajectory, such as $\mathbf{p}(p) = (p, 1)$, that interpolates between the two valid FETs at $(0, 1)$ and $(1, 1)$ and avoids the irreversible phases of this parameter space.

In general, there are two possible scenarios resulting in an irreversible phase: “intralayer” $TC_i \rightarrow TC_i$ irreversible condensations ($i = 1, 2$); and “interlayer” $TC \boxtimes TC \leftrightarrow \widetilde{CC}$ irreversible condensations. As a result of these irreversible condensations, logical qubits are measured and the \widetilde{CC} ISG is typically not recovered after such a sequence. Details of these behaviors are discussed further in Appendix G. Because of this, irreversible phases are not valid FETs: there is no well-defined automorphism since we do not return to the same \widetilde{CC} theory each period nor is the mapping bijective. Although the entanglement entropy remains in an area law phase, the topological order is no longer necessarily that of a \widetilde{CC} model.¹⁸ Once the ISG has been disrupted in these ways, we cannot always return to the \widetilde{CC} model without “resetting”, such as by projecting the system onto a trivial product state and re-measuring the original $CC \boxtimes CC$ stabilizers.

We saw in Section IV B that two FETs with automorphisms of different parity on $S_3 \times S_3$ cannot be connected. However, it is possible to construct an m -component disorder model with a trajectory that joins the two FETs. These trajectories must necessarily traverse a parameter space with irreversible phases in some corners (otherwise, we could proceed corner to corner via 1-parameter transitions thus the FETs would be connected). For example,

¹⁸ Consecutively condensing two anyons from the same layer that braid trivially, for example, may reduce the system to a vacuum $\boxtimes TC$ equivalent order.

consider the following 2-component disorder model:

$$\begin{aligned}
\widetilde{CC} &\rightarrow \begin{array}{|c|c|c|} \hline 1 & & \\ \hline & & \\ \hline 2 & & \\ \hline \end{array} \rightarrow \begin{array}{|c|c|c|} \hline & & \\ \hline & & 2 \\ \hline & & \\ \hline \end{array} \rightarrow \begin{array}{|c|c|c|} \hline & & \\ \hline & & 1 \\ \hline & & \\ \hline \end{array} \\
&\hspace{10em} \underbrace{\hspace{10em}}_{p_1} \\
&\rightarrow \begin{array}{|c|c|c|} \hline 2 & & \\ \hline & & \\ \hline & & \\ \hline \end{array} \rightarrow \widetilde{CC}. \quad (26) \\
&\hspace{10em} \underbrace{\hspace{10em}}_{p_2}
\end{aligned}$$

The corners of the 2-dimensional parameter space are furnished by

	p_1				
p_2	/		0		1
0			$(rz)(gx)(by)$		IrrP
1			IrrP		$(rybz)(gx)$

(27)

containing two interlayer irreversible phases indicated by “IrrP”. The trajectory $\mathbf{p}(p) = (p, p)$ maps from an $S_3 \times S_3$ even-parity automorphism at $p = 0$ to an odd-parity automorphism at $p = 1$. Because of these irreversible phases, there exists at least one $p' \in [0, 1]$ such that a system evolving under this trajectory will not be in an FET in the thermodynamic limit.

This shows that there are m -component disorder models with FETs that are not connected. There also exist length- m sequences of connected FETs that cannot be made into an m -component disorder model; Appendix F discusses an example. This difference arises because a sequence of connected FETs allows for an FET to have different measurement sequences for each 1-component disorder model with which it is involved. An m -component disorder model, however, must have a consistent measurement sequence and each dimension of the parameter space allows one condensation to be added or removed. If we were to extend the disorder model definition to allow for a measurement sequence involving intermediary \widetilde{CC} stages, such as $\widetilde{CC} \rightarrow \mathcal{A}_1 \rightarrow \dots \rightarrow \widetilde{CC} \rightarrow \mathcal{B}_1 \rightarrow \dots \rightarrow \widetilde{CC}$, then it becomes possible for any length- m adjacency sequence to form an m -component disorder model.¹⁹ This freedom, however, means that there is no longer a direct interpretation of disorder models as interpolations between the measurement sequences of different FETs; they are more akin to stacks of multiple temporal domain walls.

¹⁹ Specifically, if $\{A_0, A_1, \dots, A_m\}$ is an adjacency sequence (cf. Definition 2), we can construct the m -component disorder model by beginning with the measurement sequence for A_0 . Once returned to \widetilde{CC} , we append the 1-component disorder model with automorphisms id for $p_1 = 0$ and τ_{10} for $p_1 = 1$. Repeating this for all $\tau_{i(i-1)}$ up to $i = m$ gives the required m -component disorder model. This is similar to the procedure in Eq. (20), but now the freedom to return to \widetilde{CC} allows us to concatenate multiple 1-component disorder models.

The results for logically-connected FETs can also be readily modified to trajectories: we call a trajectory logically-protected if there exists a consistent nonzero-dimensional logical Hilbert subspace that remains unmeasured in the limit of $t \rightarrow \infty$ periods at any point $p \in [0, 1]$ of the trajectory. If two FETs are joined by a logically-protected trajectory, they must also be logically-connected. For component $m \geq 2$ systems, this now allows not only $\tau_{BA} \in \mathcal{C}\{(c\sigma)(c\sigma)(c\sigma)\}$ domain walls, but by Eq. (21) also $\tau_{CA} \in \mathcal{C}\{(ccc)(\sigma\sigma\sigma)\}$ when $p_i \notin \{0, 1\}$ for at least two coordinates. These τ_{CA} boundaries have $\log_2 \mathcal{D}^2 = 2$; the nontrivial anyons that localize are the three fermions from one of the F or F' groups, and the protected logical algebra is again given by either Table II or III. If the trajectory is not logically-protected, then we get τ in other conjugacy classes with $\log_2 \mathcal{D}^2 > 2$; anyons beyond the three fermions in F or F' are measured, $\text{IMS} = 0$, and there is now no protected logical subspace at criticality (which now occurs when any of the m coordinates of \mathbf{p} equals p_c). This is consistent with $\mathcal{C}\{(c\sigma)(c\sigma)(c\sigma)\}$ and $\mathcal{C}\{(ccc)(\sigma\sigma\sigma)\}$ being the sole (nontrivial) conjugacy classes with automorphisms that have invariant mutual-semion pairs.

An m -component disorder model containing an irreversible phase must support a trajectory that is not logically-protected. In order for all possible trajectories within an m -component disorder model to be logically-protected, we require that:

- (1) the enacted automorphisms have even parity on the subgroup $S_3 \times S_3$;
- (2) all corners of the hypercube in parameter space are FETs consisting of reversible sequences of condensations; and
- (3) all pairs of FETs satisfy Eq. (21) if their locations differ by an even Manhattan distance,²⁰ or Eq. (22) if an odd Manhattan distance.

Analysing competing automorphisms in this way reveals key structure about the nature of disorder in the DA color code. For example, disorder models that contain only logically-protected trajectories support a 2-qubit logical subspace that is entirely immune to the disorder. Moreover, these trajectories allow us to smoothly interpolate the measurement sequence of one FET into that of another. As noted in Section IV C, we cannot distinguish two points $p, \tilde{p} \in [0, 1]$ in a logically-protected trajectory solely using the time evolution of an observable from the protected algebra. This means that an ‘‘adiabatic transition’’ where a system evolves between two FETs using a time-dependent trajectory $p(t) = t/T \in [0, 1]$ for $t = 0, 1, \dots, T$ will not affect the periodic behavior of any logical operator that is protected. Observables that

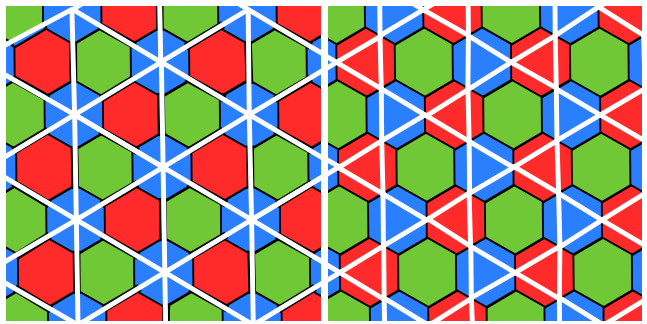


Figure 10. Left. In a model with blue links disordered, we contract the remaining green and red links to a point to form a triangular superlattice (shown in white). Spanning domain walls are equivalent to percolating bonds on this superlattice. Right. In a model with blue and red links disordered, we contract the remaining green links to a point to form a kagome superlattice (shown in white).

belong to not protected qubits, however, can distinguish these two phases. This allows us to detect phase transitions between different FETs and determine their critical behavior. This is discussed in the following section.

V. PHASE TRANSITIONS AND CRITICAL BEHAVIOUR

In Section III we argued that the behavior of competing automorphisms is governed by the formation of temporal domain walls with noncontractible boundaries. In this section we formalize this by linking the critical behavior to the universality class of bond percolation. We then perform numerical simulations to illustrate these behaviors using trajectories in an example m -component disorder model.

In a 1-component disorder model, links of one color are selected randomly. We thus contract each of the other two colored links to a point to consider only the behavior of the disordered links. In the honeycomb lattice, this contraction leaves behind the bonds of a triangular superlattice, cf. Fig. 10. Each bond is chosen independently with the same probability, and a temporal domain wall containing a contiguous region extending around a noncontractible cycle is in direct correspondence to the existence of spanning clusters of these chosen bonds. Therefore, the critical behavior of a 1-component disorder model is expected to be in the same universality class as bond percolation on a triangular lattice with a critical parameter $p_{c,\text{triangular}} = 0.347\dots$ and exponent $\nu = 1.3$ [82, 83].

In a general m -component disorder model, more complicated behaviors emerge. Disordered links in different CC layers operate independently of each other, and therefore it is possible for multiple triangular-bond percolation problems to occur concurrently, potentially with

²⁰ The Manhattan distance is the sum of the component-wise (absolute) differences between two \mathbf{p} vectors.

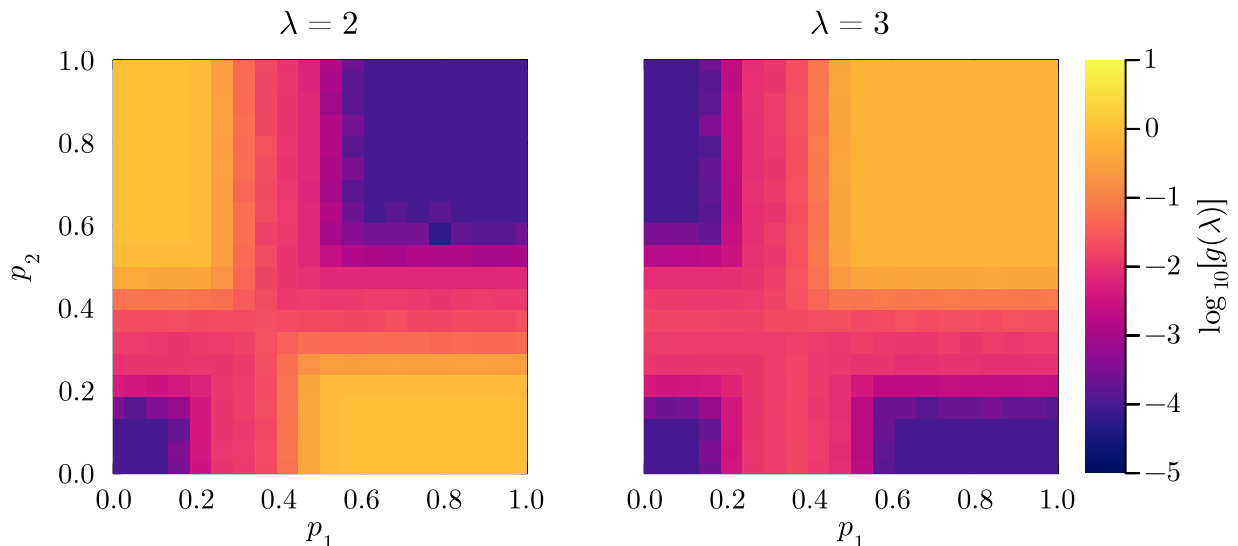


Figure 11. π and $2\pi/3$ ($\lambda = 2$ and $\lambda = 3$) Fourier components of the average-squared-expectation of the \bar{X}_3 logical operator computed from an initial logical state of $|++++\rangle$ and evolving under Eq. (23) for $t \leq 96$ time steps. This initial state and observable were chosen to demonstrate the different FETs at the corners of the parameter space. We see nonzero period-2 oscillations in the $(p_1, p_2) = (0, 1)$ and $(1, 0)$ corners, and nonzero period-3 oscillations in the $(1, 1)$ corner, consistent with the predicted automorphisms, cf. Eqs. (24), (31), (32), and (33).

different probability parameters dependent on the point in parameter space. If two different-colored links on the same layer are in consecutive disordered stages, however, then the universality class changes. Now, we contract only the one set of non-disordered links, and consider the spanning set of both disordered colors. These form the bonds of a kagome superlattice, cf. Fig. 10. If both colors are chosen independently with the same probability, then the critical behavior now is expected to follow the universality class of bond percolation on a kagome lattice with critical parameter $p_{c,\text{kagome}} = 0.524\dots$ and exponent $\nu = 1.3$ [82, 83]. We note that these same two percolation behaviors can be applied to, and were indeed observed in, the disordered honeycomb Floquet code with missing measurements [43]. In our model, the increased parameter space enables combinations of both percolation problems to arise concurrently.

We now provide evidence for these claims by performing numerical simulations of disordered DA color codes. This analysis was done in Julia, using the QuantumClifford.jl package [84] for efficient computation with the stabilizer formalism [2, 12, 79, 85]. Unless specified otherwise, simulations were repeated $N = 508$ times using a lattice with linear system size $L = 18$.

We use two metrics: firstly, the Fourier components of the average-squared-expectation of an observable O for a given initial state $|\psi\rangle$:

$$g_{O,|\psi\rangle}(\lambda) = \lim_{T \rightarrow \infty} \frac{2}{T} \sum_{t=0}^{T-1} e^{2i\pi t/\lambda} G_{O,|\psi\rangle}(t) \quad (28)$$

where

$$G_{O,|\psi\rangle}(t) = \overline{\langle \psi(t) | O | \psi(t) \rangle^2} \quad (29)$$

and $\psi(t)$ is the evolution of the initial state after an integer $t \geq 0$ periods of a given measurement sequence. We can use $g(\lambda)$ to distinguish between the subcritical and supercritical phases of a trajectory by choosing a state and observable that evolve differently under the automorphisms at the two endpoints. For example, a 3-cycle automorphism at $\mathbf{p}(0)$ and a 2-cycle automorphism at $\mathbf{p}(1)$ can result in a nonvanishing $g(3)$ when $p = 0$ and a nonvanishing $g(2)$ when $p = 1$. In practice, we need to truncate the limit at some finite T' that must be a multiple of the periods under study; this ensures that the Fourier decomposition equation is valid. We chose $T' = 96$ for our simulations: a multiple of 2, 3, 4, and 6.

Secondly, we consider the purification dynamics of the system. We track the evolution starting from a maximally-mixed logical state ρ by measuring its (average) von Neumann entropy $S = -\rho \log \rho$ over time [86]. At $t = 0$, we start from the maximum 4. Over multiple periods of the measurement sequence, entropy reduces if logical qubits are measured. A logically-protected trajectory must retain $S(t) > 0$ in the limit $t \rightarrow \infty$ at all points p . To model this, we assume the form

$$S(t) = S_\infty + (S_0 - S_\infty)e^{-\Gamma t} \quad (30)$$

and consider the decay rate Γ or associated timescale $\tau = 1/\Gamma$. We again truncate using $t \leq 96$ to approximate S_∞ and τ in numerical simulations.

We consider now an example of a 2-component disorder model. Specifically, take the measurement sequence given by Eq. (23) with automorphisms in Eq. (24). All corners of the 2-dimensional parameter space are FETs, and the associated automorphisms are even-parity on the $S_3 \times S_3$ subgroup. We choose $|\psi\rangle$ such that it is an eigen-

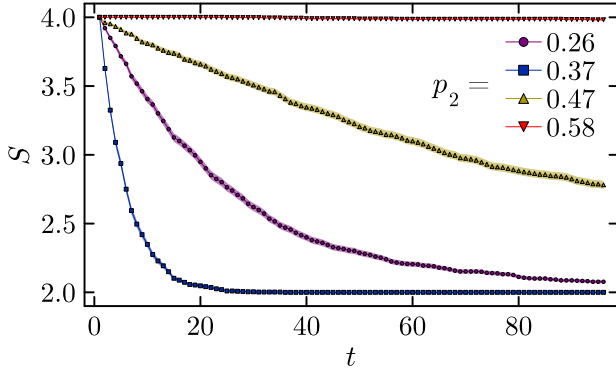


Figure 12. Average von Neumann entropy $S = \rho \log \rho$ of a maximally-mixed logical state with $S_0 = 4$ and evolving under Eq. (23) at various values of p_2 with $p_1 = 0$ (thus reducing to a 1-component disorder model). Ribbon shows the standard error of the mean based on $N = 508$ repetitions. Near the critical value of $p_c = 0.347\dots$, the entropy approaches the long-term value of $S_\infty = 2$. Away from there, the entropy remains at $S = 4$.

state of logical operators that evolve differently in the corners of the phase diagram. This is easily observed using the stabilizer picture [87]; take $\bar{X}_3 = \bar{O}[\mathbf{bx}]_h$, for example. It does not change when evolving under the identity. Under $(rx)(gy)(bz)$ we see

$$\bar{O}[\mathbf{bx}]_h \mapsto \bar{O}[\mathbf{rz}]_h \mapsto \bar{O}[\mathbf{bx}]_h \mapsto \dots \quad (31)$$

while under $(rz)(gx)(by)$ it evolves as

$$\bar{O}[\mathbf{bx}]_h \mapsto \bar{O}[\mathbf{gy}]_h \mapsto \bar{O}[\mathbf{bx}]_h \mapsto \dots \quad (32)$$

Finally, under $(rgb)(xzy)$ we get

$$\bar{O}[\mathbf{bx}]_h \mapsto \bar{O}[\mathbf{rz}]_h \mapsto \bar{O}[\mathbf{gy}]_h \mapsto \bar{O}[\mathbf{bx}]_h \mapsto \dots \quad (33)$$

Notably, it returns to an eigenstate of \bar{X}_3 only after 2 Floquet periods in $(rx)(gy)(bz)$ and $(rz)(gx)(by)$, and after 3 periods in $(rgb)(xzy)$. At other times the operator maps to \bar{Y} or \bar{Z} , and the expectation of \bar{X}_3 is 0. Starting in a $+1$ -eigenstate of $\bar{X}_1, \bar{X}_2, \bar{X}_3$, and \bar{X}_4 (denoted $|++++\rangle$), the squared expectation of \bar{X}_3 should show period-doubling oscillations between 1 and 0 at $\mathbf{p} = (0, 1)$ and $(1, 0)$, and period-tripling behavior at $\mathbf{p} = (1, 1)$. The Fourier components of $G_{\bar{X}_3, |++++\rangle}$ are plotted in Fig. 11, with nonvanishing values of $g(2)$ and $g(3)$ appearing only in these predicted corners.

These automorphisms in Eq. (24) satisfy the conditions in Section IV C and therefore it is possible for there to exist a logically-protected trajectory through the parameter space. We first plot the purification dynamics in Fig. 12, for illustrative values of \mathbf{p} . As expected from Section III, two logical qubits are measured out near the critical point, which we find to be around $p \sim 0.37$. Taking a parameter sweep of all $p_1, p_2 \in [0, 1]$, we get Fig. 13 that shows the average purification decay rate $\tau = 1/\Gamma$. Near the critical lines $p \sim 0.35$, we get a finite decay rate, with

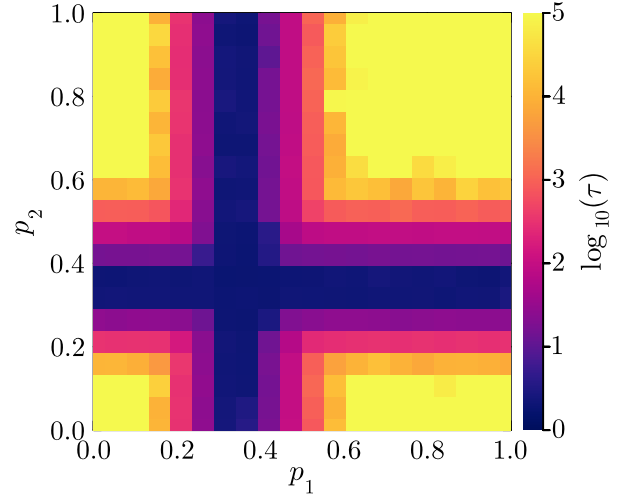


Figure 13. Average purification timescale $\tau = 1/\Gamma$ from Eq. (30) for a maximally-mixed logical state with $S_0 = 4, S_\infty = 2$ evolving under Eq. (23) at various values of p_1, p_2 , up to $t \leq 96$. Exactly 2 logical qubits are measured out when tuned near the critical lines at $p_c \sim 0.35$ (dark blue regions).

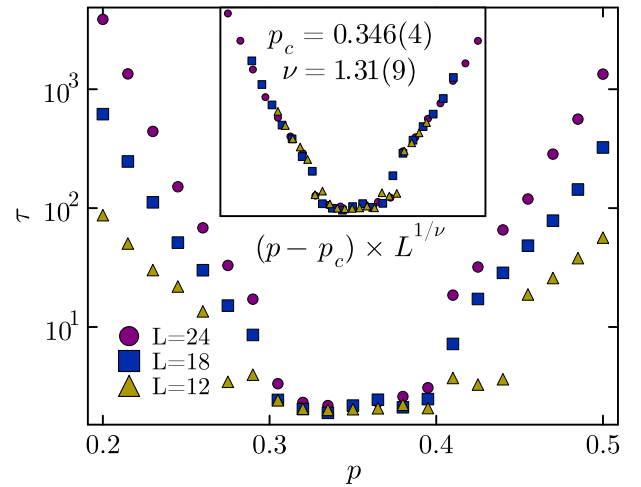


Figure 14. Average purification timescale τ for a maximally-mixed logical state evolving under Eq. (23) with the trajectory $\mathbf{p}(p) = (0, p)$ near the critical point. We run the simulation at various values of linear system size, L . Inset shows the finite-size scaling collapse under the estimated parameters of $p_c = 0.346(4)$ and $\nu = 1.31(9)$ using the functional form $(p - p_c)L^{1/\nu}$. These are consistent with the theoretical $p_c = 0.347\dots$ and $\nu = 1.3$ for bond percolation on the triangular lattice.

$\tau \rightarrow \infty$ elsewhere. To determine this critical value more precisely, we take the trajectory $\mathbf{p}(p) = (0, p)$. Figure 14 shows the average purification dynamics at different values of linear system size L , and presents a scaling-collapse of the form $(p - p_c)L^{1/\nu}$ that shows scale-invariant behaviour [43]. Using finite size scaling methods [82], we estimate critical values of $p_c = 0.346(3)$ and $\nu = 1.31(9)$,

consistent with the theoretical values for bond percolation on a triangular lattice [83].

VI. CONCLUSIONS AND OUTLOOK

We have described how competing automorphisms arise from multiple temporal domain walls partitioning a manifold, and naturally introduce disorder to the notion of Floquet-enriched topological order. By analyzing the evolution of the logical subspace and anyons, we have characterized the effect of this competition for general Abelian-anyon FETs. The number of nontrivial anyons that localize at the automorphism boundaries—equal to \mathcal{D}^2 where \mathcal{D} is the quantum dimension of the twist associated to the transition map between the neighboring automorphisms—determines the number of nontrivial logical operators that may be measured during one period of competition. The number of mutual-semions that are invariant under this transition map, IMS, indicates the number of logical qubits that are unaffected by any such logical measurement over one period. For a code with k logical qubits, these properties satisfy $\log_2 \mathcal{D}^2 + \text{IMS} \leq k$.

Using the DA color code [26] as an example, we introduced a microscopic disorder model that realizes this behavior. By tuning the disorder parameters, a system transitions between different FETs, separated by a critical point wherein $\log_2 \mathcal{D}^2$ qubits of logical information are measured and IMS are guaranteed to not be measured each period. We argued that the critical behavior of this disorder model is in the same universality class as bond percolation on triangular or kagome lattices. This picture is consistent with our numerical estimates of the critical parameters using the average purification timescale.

Our perspective of competing automorphisms has allowed us to chart the topology of the parameter space of DA color code FETs. For example, two FETs, A and B with automorphisms φ_A and φ_B , can compete using a disorder model with one random measurement stage (a “1-component disorder model”) if and only if the transition map $\varphi_B \varphi_A^{-1}$ is in the conjugacy class $\mathcal{C}\{(\mathcal{C}\sigma)(\mathcal{C}\sigma)(\mathcal{C}\sigma)\}$ of automorphisms that reflect the anyons of the color code magic square about a diagonal mirror line. We presented additional conditions that restrict the ability for two competing automorphisms to support a consistent nonzero-dimensional logical subspace that remains unmeasured over multiple periods.

Important open questions remain about disorder in the DA color code, such as the interplay between competing automorphisms and open boundaries or lattice defects [23, 70]. It remains to be seen how the effectiveness of the code’s error-correction capabilities (such as the existence of a threshold, fault-tolerance, or decoders) is affected by competing automorphisms. Future work should also consider the effect of more general disorder models, such as with weak measurements [15], interspersed random unitaries [88], coherent errors [89], or single-qubit measurements [43, 56, 90]. We expect our perspective

of competing automorphisms to be potentially useful in any disorder model that realizes spatiotemporally heterogeneous domain walls.

Moving beyond the DA color code, this work is a first step towards understanding general dynamical TOs that can support multiple automorphisms. Although we focused on FETs on a 2-torus, our results are readily generalizable to other manifolds by considering their noncontractible cycles. Future works could investigate other TOs, including microscopic models for those with Abelian anyons beyond mutual-semions, and general features of competing automorphisms in non-Abelian anyon theories [65, 91] or fracton Floquet phases [33, 92]. It would be also interesting to study what competing automorphisms can reveal about FETs evolving under unitary dynamics instead of measurements [33, 39, 40].

ACKNOWLEDGMENTS

This research was supported by the Gates Cambridge Trust and by EPSRC grant EP/V062654/1.

Appendix A: Color Code Fermions

In the color code, there are 6 fermions. These can be written as a unique fusion product of three mutual-semions:

$$\begin{array}{cc} \text{ry} \times \text{bx} \times \text{gz} & \text{ry} \times \text{bz} \times \text{gx} \\ \text{bz} \times \text{gy} \times \text{rx} & \text{bx} \times \text{gy} \times \text{rz} \\ \underbrace{\text{gx} \times \text{rz} \times \text{by}}_F & \underbrace{\text{gz} \times \text{rx} \times \text{by}}_{F'} \end{array} \quad (\text{A1})$$

The fermions form two groups, F and F' . Fermions within F are mutual-semions with fermions from F and braid trivially with those from F' , and vice versa. These products can also be summarized in the fermion magic square [26]:

$$F \left\{ \begin{array}{c|c|c} \text{ry} & \text{bx} & \text{gz} \\ \text{bz} & \text{gy} & \text{rx} \\ \text{gx} & \text{rz} & \text{by} \end{array} \right. \quad (\text{A2})$$

F'

such that the product of the three anyons in a row or column give fermions in F and F' respectively. In contrast to the magic square [cf. Eq. (2)] where anyons in the same row or column braid trivially, anyons in the same row or column of the fermion magic square are mutual-semions. Anyons not sharing a row or column braid trivially. These fermions can also be (non-uniquely) formed

from the fusion of just two mutual-semions:

$$\begin{aligned}
& \text{gx} \times \text{bz} \equiv \text{gy} \times \text{rz} \equiv \text{rx} \times \text{by} \\
& \text{bx} \times \text{rz} \equiv \text{by} \times \text{gz} \equiv \text{gx} \times \text{ry} \\
& \underbrace{\text{rx} \times \text{gz} \equiv \text{ry} \times \text{bz} \equiv \text{bx} \times \text{gy}}_F \\
& \hspace{10em} (A3) \\
& \text{bx} \times \text{gz} \equiv \text{by} \times \text{rz} \equiv \text{rx} \times \text{gy} \\
& \text{rx} \times \text{bz} \equiv \text{ry} \times \text{gz} \equiv \text{gx} \times \text{by} \\
& \underbrace{\text{gx} \times \text{rz} \equiv \text{gy} \times \text{bz} \equiv \text{bx} \times \text{ry}}_{F'}
\end{aligned}$$

In the main text, we stated a lemma about whether the groups F and F' are closed under automorphisms. We provide a proof of this lemma now:

Proof of Lemma 2. The automorphism that is trivial on $S_3 \times S_3$ and nontrivial on S_2 is the color-flavor reflection $(rx)(gy)(bz)$. On the fermion magic square [Eq. (A2)], this automorphism acts as a reflection about a horizontal mirror line through rx , gy , and bz ; this reflection does not change the fermion group. It is therefore sufficient to examine the action only on the $S_3 \times S_3$ component of an automorphism. We first consider the simplest such nontrivial automorphisms, the 2-cycles (cc) or $(\sigma\sigma)$. These act as a reflection on the fermion magic square about diagonal or antidiagonal mirror lines (considering the square on a 2-torus). A fermion in F thus maps to one in F' and vice versa as the rows and columns are interchanged. Any general even-parity (odd-parity) permutation is an even (odd) product of 2-cycles, swapping F and F' an even (odd) number of times. Therefore, the even-parity $S_3 \times S_3$ automorphisms do not swap F and F' , while odd-parity automorphisms do. \square

We also stated a lemma on the localized anyons for parallel reflections in $\mathcal{C}\{(c\sigma)(c\sigma)(c\sigma)\}$. We provide the proof here:

Proof of Lemma 3. If two automorphisms $\tau_1, \tau_2 \in \mathcal{C}\{(c\sigma)(c\sigma)(c\sigma)\}$ are equal, then their localized anyons are the same. If they are instead interpreted geometrically as reflections about inequivalent parallel lines of the magic square (on a 2-torus), then their mirror lines do not intersect, and therefore their constituent 2-cycles $(c\sigma)$ are all different (since the mirror line for $(c_1\sigma_1)(c_2\sigma_2)(c_3\sigma_3)$ is precisely the line through anyons $c_1\sigma_1$, $c_2\sigma_2$ and $c_3\sigma_3$). Moreover, the product of these three anyons— $c_1\sigma_1 \times c_2\sigma_2 \times c_3\sigma_3$ —is precisely the fermion that localizes at the twist for the automorphism. Therefore, the two fermions that localize at τ_1 and τ_2 respectively occupy distinct rows (or columns) of the fermion magic square, and are thus in the same fermion group. On the other hand, if the automorphisms have perpendicular mirror lines, then their $c\sigma$ labels intersect at some point on the magic square such that the localized fermions have one shared label, and thus are in different fermion groups. \square

Appendix B: Group Theory

1. Group Theory Essentials

In this section we briefly outline some ideas from group theory that are relevant for our discussions of the automorphism group in Appendix B 2.

We first outline general group properties, starting with group products. For a group G , a subgroup $N \triangleleft G$ is normal if and only if $gng^{-1} \in N$ for all $g \in G$ and $n \in N$. That is, elements of N are invariant under conjugation by all elements of G , or equivalently the left and right cosets gN and Ng are equal for all $g \in G$. When G is a semidirect product, written as $G = N \rtimes H$, and where N is normal in G but H may not be, then for every $g \in G$, there are unique $n \in N$ and $h \in H$ such that $g = nh$.

For a group G and two elements $a, b \in G$, if $b = gag^{-1}$ for some $g \in G$, then a and b are conjugate. Conjugacy is an equivalence relation that partitions G into conjugacy classes, denoted as

$$\mathcal{C}_a = \{gag^{-1} | g \in G\} \quad (B1)$$

for some representative $a \in G$. All elements belonging to the same conjugacy class have the same order, the minimal k such that $a^k = \text{id}$.

We now consider specifically the permutation group, S_n , which is the group of re-orderings of a set of n elements. We write these permutations using cycle notation. For example, labelling the n elements as a, b, \dots, n , the permutation $(ade)(fg)$ indicates the map $a \mapsto d \mapsto e \mapsto a$, $f \mapsto g \mapsto f$, with the other elements unchanged. A cycle is a closed mapping, such as (ade) or (fg) . The order (or length) of a cycle can be read off as the number of elements listed; a cycle of length k is called a k -cycle. (ade) is a 3-cycle, for example. A cycle is defined as having even (odd) parity if it can be written as an even (odd) number of 2-cycles. For example, $(ade) = (ad)(de)$ and therefore is even parity. Equivalently, a k -cycle is even (odd) if $k - 1$ is even (odd). A permutation can be written in multiple ways: $(ade)(fg)$ is the same as $(gf)(dea)$. However, the number and lengths of disjoint cycles forming a permutation are a fixed property of that permutation [93]. The ‘‘cycle type’’ of a permutation is written in bracket notation as

$$[1^{\alpha_1} 2^{\alpha_2} \dots n^{\alpha_n}] \quad (B2)$$

where α_k is its number of disjoint k -cycles. For example, $(ade)(fg)$ has cycle type $[2^1 3^1]$ (with $\alpha_k = 0$ omitted for brevity). Notably, the conjugacy classes of a permutation group are characterized by its elements all having the same cycle type [93].

2. Automorphism Group Essentials

In this section we apply the previous group-theory ideas to the automorphism group of the color code,

$\text{Aut}[CC]$. Concretely, $\text{Aut}[CC]$ is the group of permutations of the anyons of the color code that preserve the relationships and structure of the anyons. That is, mutual-statistics, self-statistics, and fusion rules must remain equivalent after applying $\varphi \in \text{Aut}[CC]$ to all anyons. We can represent any automorphism by a relabelling of the 6 color and flavor labels, r, g, b, x, y, z , since all c -colored or σ -flavored anyons must transform equally in order to maintain their mutual statistics and fusion rules. $\text{Aut}[CC]$ is therefore a subgroup of S_6 . We represent its elements using cycle notation, such as $(rbg)(xy)$. When color and flavor are interchanged, we have cycles such as $(rxgy)(bz)$; although the standalone map $r \mapsto x$ is ill-defined, the construction of each anyon in terms of both a color and a flavor ensures that as long as all the cycles either alternate colors and flavors, or have disjoint color-only and flavor-only cycles, the anyon mapping is valid. This cycle, for example, maps $rx \mapsto gx$ as $r \mapsto x, x \mapsto g$. A cycle such as (rxg) is not in $\text{Aut}[CC]$ for this reason.

As with the permutation groups, $\text{Aut}[CC]$ can be partitioned into conjugacy classes; Table I lists the 9 conjugacy classes and their cycle types. These are subsets of the S_6 conjugacy classes and are generated by and closed under conjugation with elements from $\text{Aut}[CC]$.

Automorphisms in $\text{Aut}[CC]$ can be identified by the decomposition into subgroups $(S_3 \times S_3) \rtimes S_2$, representing the S_3 group of 3! color (magic square row) permutations, the S_3 group of 3! flavor (magic square column) permutations, and the S_2 group of 2 color-flavor exchanges [24, 26]. Specifically, the S_2 corresponds to a reflection about the mirror line through the $rx - gy - bz$ diagonal. In cycle notation, the nontrivial element of S_2 [with trivial $(S_3 \times S_3)$ contribution] is $(rx)(gy)(bz)$. $(S_3 \times S_3)$ is closed under conjugation and hence is a normal subgroup. S_2 , on the other hand, is not. For example,

$$(rb) \cdot (rx)(gy)(bz) \cdot (rb)^{-1} = (rz)(gy)(bx). \quad (\text{B3})$$

Hence, we use the semidirect product \rtimes . To identify whether an element has nontrivial S_2 contribution, we note that for this there must be alternating color-flavor labels in the cycle notation: $(rbg)(xy)$ is trivial on S_2 while $(rxbygz)$ is not.

An important concept in Section IV B is the parity of an automorphism on the subgroup $(S_3 \times S_3)$. To identify this, we first trivialize any S_2 contribution by composing the automorphism with $(rx)(gy)(bz)$ if it has alternating color-flavor labels. We then multiply the parity of the resulting automorphism's disjoint cycles. For example, $(ry)(gz)(bx)$ involves a color-flavor reflection and therefore we modify it by

$$(rx)(gy)(bz) \cdot (ry)(gz)(bx) = (rgb)(xzy), \quad (\text{B4})$$

which results in a $[3^2]$ automorphism with net even \times even = even parity.²¹ Table I lists these parities for all

²¹ Equivalently, it can be written as an even number of 2-cycles, $(rg)(gb)(xz)(zy)$

conjugacy classes of $\text{Aut}[CC]$.

Appendix C: Localized Anyons

In Section III, we introduced the notion of localized anyons around the boundaries or twists of domain walls. Lemma 1 was used to determine the presence of operators that are protected during an evolution under multiple temporal domain walls. We prove that lemma here:

Proof of Lemma 1. We first show that if $\mathbf{b} = \tau(\mathbf{b})$ for some automorphism τ and anyon \mathbf{b} , then \mathbf{b} braids trivially with all \mathbf{c} that localize at τ . For any such anyon \mathbf{c} that localizes, there exists an \mathbf{a} such that $\mathbf{c} = \mathbf{a} \times \tau(\bar{\mathbf{a}})$. Now, the composite anyon $\mathbf{a} \times \bar{\mathbf{a}}$ is equivalent to the vacuum $\mathbf{1}$, and therefore it braids trivially with \mathbf{b} . We can write this as

$$\exp(2i\theta_{\mathbf{b},\mathbf{a}}) \exp(2i\theta_{\mathbf{b},\bar{\mathbf{a}}}) = 1 \quad (\text{C1})$$

where $\exp(2i\theta_{\mathbf{a},\mathbf{b}})$ encodes the phase factor accumulated when clockwise encircling an \mathbf{a} with \mathbf{b} (or vice versa):

$$\begin{array}{c} \begin{array}{cc} \text{a} & \text{b} \\ \text{a} & \text{b} \end{array} \\ \uparrow t \\ \text{a} & \text{b} \end{array} = e^{2i\theta_{\mathbf{b},\mathbf{a}}} = e^{2i\theta_{\mathbf{a},\mathbf{b}}} \quad (\text{C2})$$

Since τ is an automorphism, it preserves these mutual statistics and so

$$\begin{aligned} 1 &= \exp(2i\theta_{\mathbf{b},\mathbf{a}}) \exp(2i\theta_{\tau(\mathbf{b}),\tau(\bar{\mathbf{a}})}) \\ &= \exp(2i\theta_{\mathbf{b},\mathbf{a}}) \exp(2i\theta_{\mathbf{b},\tau(\bar{\mathbf{a}})}) \\ &= \exp(2i\theta_{\mathbf{b},\mathbf{a} \times \tau(\bar{\mathbf{a}})}) \\ &= \exp(2i\theta_{\mathbf{b},\mathbf{c}}) \end{aligned} \quad (\text{C3})$$

where we used $\mathbf{b} = \tau(\mathbf{b})$ and that $2(\theta_{\mathbf{b},\mathbf{a}} + \theta_{\mathbf{b},\tau(\bar{\mathbf{a}})})$ is the phase accumulated by \mathbf{b} encircling $\mathbf{a} \times \tau(\bar{\mathbf{a}}) = \mathbf{c}$. Hence, invariant anyons of τ braid trivially with all localized anyons of τ .

We next prove the reverse direction: any anyon \mathbf{b} that braids trivially with all localized anyons must be invariant. For any anyon \mathbf{a} , the anyon $\mathbf{c} = \mathbf{a} \times \tau(\bar{\mathbf{a}})$ localizes at automorphism τ , and therefore \mathbf{b} braids trivially with \mathbf{c} :

$$\exp(2i\theta_{\mathbf{b},\mathbf{c}}) = 1. \quad (\text{C4})$$

We again use the statistics-preserving property of automorphisms to write

$$\begin{aligned} 1 &= \exp(2i\theta_{\mathbf{b},\mathbf{a}}) \exp(2i\theta_{\mathbf{b},\tau(\bar{\mathbf{a}})}) \\ &= \exp(2i\theta_{\mathbf{b},\mathbf{a}}) \exp(2i\theta_{\tau^{-1}(\mathbf{b}),\bar{\mathbf{a}}}). \end{aligned} \quad (\text{C5})$$

By anyons and anti-anyons having the same mutual-statistics, $\theta_{p,q} = \theta_{\bar{p},\bar{q}}$, we have

$$\begin{aligned} 1 &= \exp(2i\theta_{\mathbf{b},\mathbf{a}}) \exp(2i\theta_{\tau^{-1}(\bar{\mathbf{b}}),\mathbf{a}}) \\ &= \exp(2i\theta_{\mathbf{d},\mathbf{a}}) \end{aligned} \quad (\text{C6})$$

where $\mathbf{d} = \mathbf{b} \times \tau^{-1}(\bar{\mathbf{b}})$. This relation holds for all anyons \mathbf{a} , meaning that there is no anyon encircling action that can distinguish \mathbf{d} from the vacuum 1 (\mathbf{d} is “transparent” [75]). For modular anyon theories, such as those formed by topological stabilizer codes, braiding is nondegenerate [65, 81], which implies that \mathbf{d} is the vacuum. That is, $\mathbf{b} = \tau^{-1}(\bar{\mathbf{b}})$ or equivalently, $\tau(\mathbf{b}) = \mathbf{b}$ as required. \square

Appendix D: Computing and Creating Automorphisms

Given a dynamical scheme of the form $\widetilde{CC} \rightarrow TC \boxtimes TC \rightarrow \dots \rightarrow TC \boxtimes TC \rightarrow \widetilde{CC}$, we compute the enacted automorphism by the formula [26]

$$\varphi_f[(rx)(gy)(bz)]^\alpha [(rz)(gy)(bx)]^\beta \varphi_i^{-1} \quad (\text{D1})$$

where φ_i and φ_f are the contributions from the $\widetilde{CC} \rightarrow TC \boxtimes TC$ and $TC \boxtimes TC \rightarrow \widetilde{CC}$ transitions respectively. Table D.I lists these for all possible reversible transitions. α is the number of reversible transitions that the first CC layer undergoes. β is the number of reversible transitions that the second CC layer undergoes.

For example, consider

$$\widetilde{CC} \rightarrow \begin{array}{|c|c|c|} \hline 1 & & \\ \hline 2 & & \\ \hline \end{array} \rightarrow \begin{array}{|c|c|c|} \hline & & \\ \hline & 1 & \\ \hline & & \\ \hline \end{array} \rightarrow \begin{array}{|c|c|c|} \hline 1 & & \\ \hline & & 2 \\ \hline \end{array} \rightarrow \widetilde{CC}. \quad (\text{D2})$$

We have that $\varphi_i = (gb)$, $\varphi_f = (xy)$, $\alpha = 2$, and $\beta = 1$. α and β are important only mod 2, since they exponent 2-cycles. This gives overall automorphism

$$(xy) \cdot \text{id} \cdot (rz)(gy)(bx) \cdot (gb)^{-1} = (rz)(gy)(bx). \quad (\text{D3})$$

On the other hand, given any automorphism $\varphi \in \text{Aut}[CC]$, it is possible to create a measurement sequence that realizes it. All 72 automorphisms and example measurement sequences are given in Ref. [26]. Moreover, it is possible to ensure that this measurement sequence ends with a particular $TC \boxtimes TC$ condensation prior to returning to \widetilde{CC} .

We summarize here the procedure described in Ref. [26]. Let $\mathcal{B}_1, \dots, \mathcal{B}_n$ be a sequence of n sets of bosons of $CC \boxtimes CC$ that form the condensations for n child theories C_1, \dots, C_n . We set $\mathcal{B}_n = \{1, \mathbf{rz}_1\mathbf{rz}_2, \mathbf{gz}_1\mathbf{gz}_2, \mathbf{bz}_1\mathbf{bz}_2\}$ such that $C_n = \widetilde{CC}$. We require that the sequence of condensations is reversible. This allows us to associate an isomorphism λ from C_1 to C_n . Let $\phi \in \text{Aut}[CC \boxtimes CC]$ be an automorphism of the parent theory such that $\phi(\mathcal{B}_1) = \mathcal{B}_1$ and $\phi(\mathcal{B}_n) = \mathcal{B}_n$.

This also defines an automorphism on C_1 and C_n ; assume we have chosen C_1 such that ϕ acts as the trivial automorphism id_1 on C_1 . On C_n it acts as $\varphi \in \text{Aut}[CC]$. The sequence of reversible condensations $\phi(\mathcal{B}_1), \dots, \phi(\mathcal{B}_n)$ now enacts the isomorphism $\varphi\lambda$ from C_1 to C_n . The sequence

$$\mathcal{B}_n, \mathcal{B}_{n-1}, \dots, \mathcal{B}_1, \phi(\mathcal{B}_2), \dots, \phi(\mathcal{B}_{n-1}), \mathcal{B}_n \quad (\text{D4})$$

therefore enacts the automorphism $\varphi\lambda\lambda^{-1} = \varphi$ on $C_n = \widetilde{CC}$. This allows us to create any automorphism $\varphi \in \text{Aut}[CC]$.

Because λ does not affect the final automorphism, we can arbitrarily specify that \mathcal{B}_{n-1} is any set of bosons as long as it creates a reversible pair of condensations with \widetilde{CC} (i.e. any of the theories in Table D.I). If we wish to end with a specific (valid) $TC \boxtimes TC$ theory with condensed bosons \mathcal{B} , we therefore specify that $\mathcal{B}_{n-1} = \phi^{-1}(\mathcal{B})$. Note that this reasoning allows us to specify only the ending or the first $TC \boxtimes TC$ theory, not both.

Appendix E: Example Disorder Models

In this section, we provide more examples of disorder models.

a. Trivial-adjacent FETs We first consider examples of 1-component disorder models that realize connections between the trivial FET (when $p = 0$) and each of the 6 automorphisms in $\mathcal{C}\{(\text{c}\sigma)(\text{c}\sigma)(\text{c}\sigma)\}$ (when $p = 1$):

$$(ry)(gx)(bz) : \quad \widetilde{CC} \rightarrow \begin{array}{|c|c|c|} \hline 1 & & \\ \hline 2 & & \\ \hline \end{array} \rightarrow \underbrace{\begin{array}{|c|c|c|} \hline & & \\ \hline & 1 & \\ \hline & & \\ \hline \end{array}}_p \rightarrow \widetilde{CC}$$

$$(rz)(gx)(by) : \quad \widetilde{CC} \rightarrow \begin{array}{|c|c|c|} \hline 1 & & \\ \hline 2 & & \\ \hline \end{array} \rightarrow \underbrace{\begin{array}{|c|c|c|} \hline & & \\ \hline & 2 & \\ \hline & & \\ \hline \end{array}}_p \rightarrow \widetilde{CC}$$

$$(ry)(gz)(bx) : \quad \widetilde{CC} \rightarrow \begin{array}{|c|c|c|} \hline 1 & & \\ \hline & & \\ \hline & & \\ \hline \end{array} \rightarrow \underbrace{\begin{array}{|c|c|c|} \hline & & \\ \hline & & \\ \hline & 1 & \\ \hline \end{array}}_p \rightarrow \widetilde{CC}$$

$$(rx)(gz)(by) : \quad \widetilde{CC} \rightarrow \begin{array}{|c|c|c|} \hline 1 & & \\ \hline 2 & & \\ \hline \end{array} \rightarrow \underbrace{\begin{array}{|c|c|c|} \hline & & \\ \hline & 2 & \\ \hline & & \\ \hline \end{array}}_p \rightarrow \widetilde{CC}$$

Table D.I. All possible isomorphism contributions from the $\widetilde{CC} \leftrightarrow TC \boxtimes TC$ reversible transitions of a dynamical scheme. Adapted from Ref. 26. There are two possible $TC \boxtimes TC$ theories for each isomorphism.

Isomorphism	Theories	Isomorphism	Theories
id	$\begin{array}{ c c } \hline 1 & \\ \hline 2 & \\ \hline \end{array}, \begin{array}{ c } \hline 1 \\ \hline 2 \\ \hline \end{array}$	(xy)	$\begin{array}{ c c } \hline 1 & \\ \hline 2 & \\ \hline \end{array}, \begin{array}{ c } \hline 1 \\ \hline 2 \\ \hline \end{array}$
(rg)	$\begin{array}{ c c } \hline 1 & \\ \hline 2 & \\ \hline \end{array}, \begin{array}{ c } \hline 1 \\ \hline 2 \\ \hline \end{array}$	$(rg)(xy)$	$\begin{array}{ c c } \hline 1 & \\ \hline 2 & \\ \hline \end{array}, \begin{array}{ c } \hline 1 \\ \hline 2 \\ \hline \end{array}$
(gb)	$\begin{array}{ c c } \hline 1 & \\ \hline 2 & \\ \hline \end{array}, \begin{array}{ c } \hline 1 \\ \hline 2 \\ \hline \end{array}$	$(gb)(xy)$	$\begin{array}{ c c } \hline 1 & \\ \hline 2 & \\ \hline \end{array}, \begin{array}{ c } \hline 1 \\ \hline 2 \\ \hline \end{array}$
(rb)	$\begin{array}{ c c } \hline 2 & \\ \hline 1 & \\ \hline \end{array}, \begin{array}{ c } \hline 2 \\ \hline 1 \\ \hline \end{array}$	$(rb)(xy)$	$\begin{array}{ c c } \hline 2 & \\ \hline 1 & \\ \hline \end{array}, \begin{array}{ c } \hline 2 \\ \hline 1 \\ \hline \end{array}$
(rgb)	$\begin{array}{ c c } \hline 2 & \\ \hline 1 & \\ \hline \end{array}, \begin{array}{ c } \hline 2 \\ \hline 1 \\ \hline \end{array}$	$(rgb)(xy)$	$\begin{array}{ c c } \hline 2 & \\ \hline 1 & \\ \hline \end{array}, \begin{array}{ c } \hline 2 \\ \hline 1 \\ \hline \end{array}$
(rbg)	$\begin{array}{ c c } \hline 2 & \\ \hline 1 & \\ \hline \end{array}, \begin{array}{ c } \hline 2 \\ \hline 1 \\ \hline \end{array}$	$(rbg)(xy)$	$\begin{array}{ c c } \hline 2 & \\ \hline 1 & \\ \hline \end{array}, \begin{array}{ c } \hline 2 \\ \hline 1 \\ \hline \end{array}$

$$(rx)(gy)(bz) : \quad \widetilde{CC} \rightarrow \begin{array}{|c|c|} \hline 1 & \\ \hline 2 & \\ \hline \end{array} \rightarrow \underbrace{\begin{array}{|c|} \hline 1 \\ \hline \end{array}}_p \rightarrow \begin{array}{|c|c|} \hline & \\ \hline & \\ \hline \end{array} \rightarrow \begin{array}{|c|} \hline 1 \\ \hline \\ \hline \end{array} \rightarrow \widetilde{CC}$$

with the corners of the parameter space supporting FETs with automorphisms

$$\begin{array}{c|cc} & p_1 & \\ \hline p_2 & 0 & 1 \\ \hline 0 & (rb)(xy) & (ryggbz) \\ \hline 1 & (rzbygx) & (xzy) \end{array}$$

$$(rz)(gy)(bx) : \quad \widetilde{CC} \rightarrow \begin{array}{|c|c|} \hline 1 & \\ \hline 2 & \\ \hline \end{array} \rightarrow \underbrace{\begin{array}{|c|} \hline 2 \\ \hline \end{array}}_p \rightarrow \begin{array}{|c|c|} \hline & \\ \hline & \\ \hline \end{array} \rightarrow \begin{array}{|c|} \hline 2 \\ \hline \\ \hline \end{array} \rightarrow \widetilde{CC}$$

Notably, there does not exist a logically-protected trajectory between $\mathbf{p} = (0, 0)$ and $\mathbf{p} = (1, 1)$ because

$$(xzy) \cdot [(rb)(xy)]^{-1} = (rb)(yz) \notin \mathcal{C}\{(ccc)(\sigma\sigma\sigma)\} \quad (\text{E1})$$

in violation of Eq. (21).

c. Example 3. This is an example of a 2-component disorder model where we have an irreversible phase in one corner, from an interlayer irreversible condensation. This differs from Eq. (26) in that all other FETs are in the same parity cluster.

b. Example 2. Secondly, consider

$$\begin{array}{l} \widetilde{CC} \rightarrow \begin{array}{|c|c|} \hline 1 & \\ \hline 2 & \\ \hline \end{array} \rightarrow \begin{array}{|c|c|} \hline & \\ \hline 1 & 2 \\ \hline \end{array} \rightarrow \underbrace{\begin{array}{|c|c|} \hline & \\ \hline & \\ \hline \end{array}}_{p_1} \\ \rightarrow \begin{array}{|c|c|} \hline & \\ \hline 2 & \\ \hline \end{array} \rightarrow \begin{array}{|c|} \hline 2 \\ \hline 1 \\ \hline \end{array} \rightarrow \widetilde{CC} \end{array}$$

$$\begin{array}{l} \widetilde{CC} \rightarrow \begin{array}{|c|c|} \hline 1 & \\ \hline 2 & \\ \hline \end{array} \rightarrow \begin{array}{|c|c|} \hline & \\ \hline 2 & \\ \hline & 1 \\ \hline \end{array} \rightarrow \underbrace{\begin{array}{|c|c|} \hline 1 & \\ \hline & \\ \hline \end{array}}_{p_1} \\ \rightarrow \begin{array}{|c|c|} \hline 2 & \\ \hline & \\ \hline \end{array} \rightarrow \widetilde{CC} \end{array}$$

The corners host FETs with automorphisms

$$\begin{array}{c|c|c} & p_1 & \\ \hline p_2 & & \\ \hline 0 & (rg)(xz) & \text{IrrP} \\ \hline 1 & (rygxbz) & (rgb) \end{array}.$$

d. Example 4. This measurement sequence demonstrates multiple automorphisms in the even-parity component; these are connected but cannot be logically-connected.

$$\begin{array}{c} \widetilde{CC} \\ \rightarrow \\ \begin{array}{c|c|c} 1 & & \\ \hline & & \\ \hline 2 & & \end{array} \\ \rightarrow \\ \begin{array}{c|c|c} & 2 & \\ \hline & & \\ \hline & 1 & \end{array} \\ \rightarrow \\ \underbrace{\begin{array}{c|c|c} & & 1 \\ \hline & & \\ \hline & & \end{array}}_{p_1} \\ \\ \rightarrow \\ \underbrace{\begin{array}{c|c|c} & & 2 \\ \hline & & \\ \hline & & \end{array}}_{p_2} \\ \rightarrow \\ \begin{array}{c|c|c} & 1 & \\ \hline & & \\ \hline & 2 & \end{array} \\ \rightarrow \\ \widetilde{CC} \end{array}$$

The automorphisms are

$$\begin{array}{c|c|c} & p_1 & \\ \hline p_2 & & \\ \hline 0 & (rg) & (rxgy)(bz) \\ \hline 1 & (rzgy)(bx) & (rbg)(xz) \end{array}.$$

Appendix F: Connected FETs

We first provide an example of two measurement sequences that both realize the same FET and automorphism, id , but are not “connected” to each other: one sequence cannot be made into the other by adding or removing condensation steps and while maintaining solely reversible transitions. The two sequences are

$$\begin{array}{c} \widetilde{CC} \\ \rightarrow \\ \begin{array}{c|c|c} 1 & & \\ \hline & & \\ \hline 2 & & \end{array} \\ \rightarrow \\ \begin{array}{c|c|c} & 1 & 2 \\ \hline & & \\ \hline & & \end{array} \\ \rightarrow \\ \begin{array}{c|c|c} 2 & & \\ \hline & & \\ \hline 1 & & \end{array} \\ \\ \rightarrow \\ \begin{array}{c|c|c} & 2 & 1 \\ \hline & & \\ \hline & 1 & \\ \hline & & 2 \end{array} \\ \rightarrow \\ \widetilde{CC} \end{array} \quad (\text{F1})$$

and

$$\begin{array}{c} \widetilde{CC} \\ \rightarrow \\ \begin{array}{c|c|c} 1 & & \\ \hline & & \\ \hline 2 & & \end{array} \\ \rightarrow \\ \widetilde{CC}. \end{array} \quad (\text{F2})$$

Let us begin with Eq. (F1) and consider for now just the first layer. We wish to add or remove condensed bosons to manipulate it into the form of Eq. (F2). The sequence of bosons $\text{rx}, \text{gy}, \text{bx}, \text{gz}, \text{rx}$ forms a path on the fermion magic square (the path can wrap around periodic boundary conditions) [26]:

$$\begin{array}{c|c|c} \text{ry} & \text{bz} & \\ \hline \text{bz} & \text{gx} & \text{rx} \\ \hline \text{gx} & \text{rz} & \text{by} \end{array} \quad (\text{F3})$$

The requirement for reversible transitions (that adjacent bosons in the sequence are mutual-semions) necessitates that these arrows only point horizontally or vertically; we must follow this rule when adding or removing condensed bosons. As such, we are never able to remove bosons that sit at the corners of the path—this would result in a diagonal arrow. We may add or remove bosons from the start or end of the sequence only if the resulting pair of layer-1 and layer-2 bosons creates a reversible transition to \widetilde{CC} ; the gz boson can never begin or end the sequence. We therefore cannot remove gz from our sequence. The same argument applies to the sequence of bosons in the second layer. It is thus impossible to connect the measurement sequence of Eq. (F1) with Eq. (F2) while maintaining reversible transitions.

Furthermore, we can also show that not every length- m adjacency sequence can be made into an m -component disorder model. We discuss here one such example.

Consider the adjacency sequence $\{A_0, \mathbb{1}, A_2\}$, where $\mathbb{1}$ is the trivial FET with automorphism id , and A_0 and A_2 have automorphisms φ_0 and $\varphi_2 \in \mathcal{C}\{(\text{c}\sigma)(\text{c}\sigma)(\text{c}\sigma)\}$ respectively [as required by the separation condition, Eq. (17)]. We wish to show that for some choice of A_0 and A_2 there is no 2-component disorder model that realizes $A_0, \mathbb{1}$, and A_2 in three of its parameter-space corners. Equivalently, there is no measurement sequence $\widetilde{CC} \rightarrow (TC \boxtimes TC)_1 \rightarrow \dots \rightarrow (TC \boxtimes TC)_k \rightarrow \widetilde{CC}$ that realizes the id automorphism and that can form both a 1-component disorder model with A_0 and a 1-component disorder model with A_2 .

Assume that we have chosen some measurement sequence for $\mathbb{1}$. Eq. (D1) tells us that

$$\text{id} = \varphi_f [(rx)(gy)(bz)]^\alpha [(rz)(gy)(bx)]^\beta \varphi_i^{-1}. \quad (\text{F4})$$

We first simplify this by noting that for all φ_i, φ_f isomorphism contributions listed in Table D.I, none contain permutations affecting the z flavor label. This enforces that $\alpha = \beta = 0$. Then, $\text{id} = \varphi_f \varphi_i^{-1}$ gives $\varphi_f = \varphi_i$. This means that the first condensation $(TC \boxtimes TC)_1$ is the same as the final condensation $(TC \boxtimes TC)_k$ in the measurement sequence.

We now consider the possible 1-component disorder models that can be made that involve our chosen measurement sequence. By Eq. (D1), there are only 6 possible effects that changing the disorder parameter from $p = 0$ to $p = 1$ (or equivalently, $p = 1$ to $p = 0$) can have on the enacted automorphism:

- (1) $\alpha \mapsto \alpha + 1 \pmod{2}$;
- (2) $\beta \mapsto \beta + 1 \pmod{2}$;
- (3) $\alpha \mapsto \alpha + 1 \pmod{2}$ and $\varphi_i \mapsto \varphi'_i$ by adding an additional condensation step in the first CC layer prior to $(TC \boxtimes TC)_1$;
- (4) $\alpha \mapsto \alpha + 1 \pmod{2}$ and $\varphi_f \mapsto \varphi'_f$ by adding an additional condensation step in the first CC layer after $(TC \boxtimes TC)_k$;

- (5) $\beta \mapsto \beta + 1 \pmod 2$ and $\varphi_i \mapsto \varphi_i''$ by adding an additional condensation step in the second CC layer prior to $(TC \boxtimes TC)_1$; and
- (6) $\beta \mapsto \beta + 1 \pmod 2$ and $\varphi_f \mapsto \varphi_f''$ by adding an additional condensation step in the second CC layer after $(TC \boxtimes TC)_k$.

We can show that these 6 options realize only 4 different automorphisms. For each of (3)-(6) there is only one choice of condensation boson that we can introduce that is a mutual-semion with the condensates before and after it. Thus, since $(TC \boxtimes TC)_1 = (TC \boxtimes TC)_k$ and $\varphi_i = \varphi_f$, we must have $\varphi_i' = \varphi_f'$ and $\varphi_i'' = \varphi_f''$. Let $\varphi_{(3)}$ be the enacted automorphism when we follow option (3),

$$\varphi_{(3)} = \varphi_i[(rx)(gy)(bz)]\varphi_i'^{-1}, \quad (\text{F5})$$

where we use $\varphi_i = \varphi_f$. Similarly, let $\varphi_{(4)}$ be the enacted automorphism for option (4),

$$\varphi_{(4)} = \varphi_i'[(rx)(gy)(bz)]\varphi_i^{-1}, \quad (\text{F6})$$

where we use $\varphi_i' = \varphi_f'$. Finally, by noting that all $\varphi \in \mathcal{C}\{(c\sigma)(c\sigma)(c\sigma)\}$ satisfy $\varphi = \varphi^{-1}$, we have

$$\begin{aligned} \varphi_{(3)} &= \varphi_{(3)}^{-1} \\ &= (\varphi_i[(rx)(gy)(bz)]\varphi_i'^{-1})^{-1} \\ &= \varphi_i'[(rx)(gy)(bz)]\varphi_i^{-1} \\ &= \varphi_{(4)}. \end{aligned} \quad (\text{F7})$$

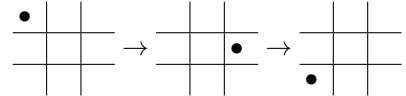
An equivalent argument shows that $\varphi_{(5)} = \varphi_{(6)}$. This means that a given measurement sequence for $\mathbb{1}$ can only be in 1-component disorder models with 4 other FETs. However, there are 6 FETs that are connected to $\mathbb{1}$ (corresponding to the 6 elements of $\mathcal{C}\{(c\sigma)(c\sigma)(c\sigma)\}$). We therefore cannot construct a 2-component disorder model with $\mathbb{1}$ and all possible A_0 and A_2 .

A more relaxed notion of connectivity may arise if we enable additional behaviors in the disorder model. As discussed in footnote 19, allowing for \widetilde{CC} stages in the middle of a condensation sequence means that any length- m adjacency sequence can now be made into an m -component disorder model. This could be generalized further to allow for any bosons of $CC \boxtimes CC$ to be condensed in the disorder model. For example, starting from \widetilde{CC} and condensing \mathbf{rx}_1 (with no boson in the second layer), then \mathbf{bx}_1 , then returning to \widetilde{CC} includes only reversible transitions (all logical operators update reversibly); this allows us to make changes to the measurement sequences in ways previously forbidden [i.e., $TC(\mathbf{rx}) \rightarrow TC(\mathbf{bx})$ is not a reversible transition]. We may also consider models with anticorrelated disorder between two link types: measuring \mathbf{rx}_1 with probability p and \mathbf{bx}_1 with probability $1 - p$, for example. Even with condensed bosons in the second layer, this would not result in an irreversible phase because the regions of \mathbf{rx} - and \mathbf{bx} -measurements do not overlap. In the case of Eq. (F1), this would allow us to remove the \mathbf{gz}_1 condensation while retaining reversible transitions, and thus Eq. (F1) and Eq. (F2) can be connected.

Appendix G: Irreversible Phases

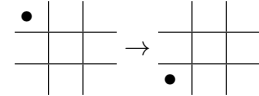
As discussed in Section IV D, irreversible phases arise in the corners of m -component disorder models when the measurement sequences create irreversible condensations. These generally result in logical information measured out due to the condensation of commuting anyons [24]. Moreover, there are also disruptions to the ISG of the code, such that we do not return to the \widetilde{CC} ISG after the period. For intralayer scenarios the plaquette operators are not reintroduced and links remain from the intermediary TC phases. For interlayer scenarios the two CC layers are not recoupled, resulting in logicals that may reside on only one layer, for example. We describe these behaviors in more detail here.

We first consider irreversible $TC \boxtimes TC$ intralayer transitions, starting from the illustrative case of child theories of CC . Measuring a link corresponding to the hopping operator for anyon $c\sigma$ has two effects on the ISG: (1) remove plaquettes of color c and flavor σ' for $\sigma' \neq \sigma$; and (2) add plaquettes of color c' and flavor σ for $c' \neq c$.²² By tracking the presence of these plaquettes at each measurement stage, we can determine if the ISG is reproduced. For example, contrast the case of



$$\begin{array}{c} \bullet \\ | \\ \hline | \\ \hline \end{array} \rightarrow \begin{array}{c} | \\ | \\ \hline | \\ \hline \bullet \end{array} \rightarrow \begin{array}{c} | \\ | \\ \hline \bullet \\ \hline | \end{array} \quad (\text{G1})$$

with



$$\begin{array}{c} \bullet \\ | \\ \hline | \\ \hline \end{array} \rightarrow \begin{array}{c} | \\ | \\ \hline \bullet \\ \hline | \end{array}. \quad (\text{G2})$$

In the following table we denote by \bullet the presence of each type of plaquette operator in the ISG at each stage of the measurement sequences. For the first example, we have:

	rx	gx	bx	rz	gz	bz
$TC(\mathbf{rx})$	\bullet	\bullet	\bullet		\bullet	\bullet
$TC(\mathbf{gz})$	\bullet		\bullet	\bullet	\bullet	\bullet
$TC(\mathbf{bx})$	\bullet	\bullet	\bullet	\bullet	\bullet	

$$(\text{G3})$$

All plaquettes are recovered as expected and we realize the $TC(\mathbf{bx})$ phase. In the second example, however, we have

	rx	gx	bx	rz	gz	bz
$TC(\mathbf{rx})$	\bullet	\bullet	\bullet		\bullet	\bullet
$TC(\mathbf{bx})$	\bullet	\bullet	\bullet		\bullet	

$$(\text{G4})$$

In this final state, there are individual rx and bx -type links, but no rz -type plaquettes. The effect of this is

²² Technically, $c\sigma$ -links are added, not plaquette terms. However, the product of $c\sigma$ links around a $c' \neq c$ hexagon is equivalent to the $c'\sigma$ -plaquette operator.

that a logical $\bar{O}(\mathbf{bz})$, for example, no longer has representatives that extend across all homologous cycles of the torus, since there are no rz -plaquettes in the ISG with which to multiply to deform one string into another.

Additional disruptions occur when we consider $TC \boxtimes TC \rightarrow \overline{CC}$ interlayer irreversible transitions. In these, we have a situation where the measured $Z_1 Z_2$ interlayer links will not always anticommute with some element of the

ISG (with the precise scenario determined by the random disorder realization). These links are therefore not added to the ISG, and we produce a phase with interlinked \overline{CC} layers that behaves differently to \overline{CC} . In particular, there exist X -logical operators that reside on just one layer, e.g. $\bar{O}(\mathbf{bx}_1)$, or Z -logical operators that cannot freely switch between the two layers as they may in \overline{CC} (wherein $\mathbf{rz}_1 \sim \mathbf{rz}_2$, for example).

-
- [1] A. M. Steane, Error Correcting Codes in Quantum Theory, *Physical Review Letters* **77**, 793 (1996).
- [2] D. E. Gottesman, *Stabilizer Codes and Quantum Error Correction*, Ph.D. thesis, California Institute of Technology (1997).
- [3] A. Yu. Kitaev, Quantum Error Correction with Imperfect Gates, in *Quantum Communication, Computing, and Measurement*, edited by O. Hirota, A. S. Holevo, and C. M. Caves (Springer US, Boston, MA, 1997) pp. 181–188.
- [4] A. Y. Kitaev, Quantum computations: Algorithms and error correction, *Russian Mathematical Surveys* **52**, 1191 (1997).
- [5] E. Knill and R. Laflamme, Theory of quantum error-correcting codes, *Physical Review A* **55**, 900 (1997).
- [6] J. Preskill, Fault-Tolerant Quantum Computation, in *Introduction to Quantum Computation and Information* (WORLD SCIENTIFIC, 1998) pp. 213–269.
- [7] P. W. Shor, Fault-tolerant quantum computation (1997), [arXiv:quant-ph/9605011](https://arxiv.org/abs/quant-ph/9605011).
- [8] E. Knill, R. Laflamme, and L. Viola, Theory of Quantum Error Correction for General Noise, *Physical Review Letters* **84**, 2525 (2000).
- [9] T. Schuster, C. Yin, X. Gao, and N. Y. Yao, A polynomial-time classical algorithm for noisy quantum circuits (2024), [arXiv:2407.12768](https://arxiv.org/abs/2407.12768).
- [10] X. G. Wen, Vacuum degeneracy of chiral spin states in compactified space, *Physical Review B* **40**, 7387 (1989).
- [11] E. Witten, Quantum field theory and the Jones polynomial, *Communications in Mathematical Physics* **121**, 351 (1989).
- [12] D. Poulin, Stabilizer Formalism for Operator Quantum Error Correction, *Physical Review Letters* **95**, 230504 (2005), [arXiv:quant-ph/0508131](https://arxiv.org/abs/quant-ph/0508131).
- [13] X. Fu and D. Gottesman, Error Correction in Dynamical Codes (2024), [arXiv:2403.04163](https://arxiv.org/abs/2403.04163) [quant-ph].
- [14] M. Davydova, N. Tantivasadakarn, and S. Balasubramanian, Floquet Codes without Parent Subsystem Codes, *PRX Quantum* **4**, 020341 (2023).
- [15] G.-Y. Zhu and S. Trebst, Qubit fractionalization and emergent Majorana liquid in the honeycomb Floquet code induced by coherent errors and weak measurements (2023), [arXiv:2311.08450](https://arxiv.org/abs/2311.08450) [cond-mat, physics:quant-ph].
- [16] M. B. Hastings and J. Haah, Dynamically Generated Logical Qubits, *Quantum* **5**, 564 (2021).
- [17] S. B. Bravyi and A. Y. Kitaev, Quantum codes on a lattice with boundary, [arXiv:quant-ph/9811052](https://arxiv.org/abs/quant-ph/9811052) (1998), [arXiv:quant-ph/9811052](https://arxiv.org/abs/quant-ph/9811052).
- [18] E. Dennis, A. Kitaev, A. Landahl, and J. Preskill, Topological quantum memory, *Journal of Mathematical Physics* **43**, 4452 (2002), [arXiv:quant-ph/0110143](https://arxiv.org/abs/quant-ph/0110143).
- [19] A. Y. Kitaev, Fault-tolerant quantum computation by anyons, *Annals of Physics* **303**, 2 (2003), [arXiv:quant-ph/9707021](https://arxiv.org/abs/quant-ph/9707021).
- [20] A. Kitaev, Anyons in an exactly solved model and beyond, *Annals of Physics* **321**, 2 (2006).
- [21] C. Vuillot, Planar Floquet Codes (2021), [arXiv:2110.05348](https://arxiv.org/abs/2110.05348) [quant-ph].
- [22] J. Haah and M. B. Hastings, Boundaries for the Honeycomb Code, *Quantum* **6**, 693 (2022), [arXiv:2110.09545](https://arxiv.org/abs/2110.09545) [quant-ph].
- [23] T. D. Ellison, J. Sullivan, and A. Dua, Floquet codes with a twist (2023), [arXiv:2306.08027](https://arxiv.org/abs/2306.08027) [quant-ph].
- [24] M. S. Kesselring, J. C. Magdalena De La Fuente, F. Thomsen, J. Eisert, S. D. Bartlett, and B. J. Brown, Anyon Condensation and the Color Code, *PRX Quantum* **5**, 010342 (2024), [arXiv:2212.00042](https://arxiv.org/abs/2212.00042) [cond-mat, physics:quant-ph].
- [25] D. Aasen, Z. Wang, and M. B. Hastings, Adiabatic paths of Hamiltonians, symmetries of topological order, and automorphism codes, *Physical Review B* **106**, 085122 (2022).
- [26] M. Davydova, N. Tantivasadakarn, S. Balasubramanian, and D. Aasen, Quantum computation from dynamic automorphism codes, *Quantum* **8**, 1448 (2024).
- [27] A. Bauer, The $x+y$ Floquet code: A simple example for topological quantum computation in the path integral approach (2024), [arXiv:2408.07265](https://arxiv.org/abs/2408.07265) [quant-ph].
- [28] J. C. M. de la Fuente, J. Old, A. Townsend-Teague, M. Rispler, J. Eisert, and M. Müller, The XYZ ruby code: Making a case for a three-colored graphical calculus for quantum error correction in spacetime (2024), [arXiv:2407.08566](https://arxiv.org/abs/2407.08566) [cond-mat, physics:math-ph, physics:quant-ph].
- [29] A. Dua, N. Tantivasadakarn, J. Sullivan, and T. D. Ellison, Engineering 3D Floquet Codes by Rewinding, *PRX Quantum* **5**, 020305 (2024).
- [30] O. Higgott and N. P. Breuckmann, Constructions and performance of hyperbolic and semi-hyperbolic Floquet codes (2023), [arXiv:2308.03750](https://arxiv.org/abs/2308.03750) [quant-ph].
- [31] H. Bombin, Topological subsystem codes, *Physical Review A* **81**, 032301 (2010).
- [32] D. Aasen, J. Haah, Z. Li, and R. S. K. Mong, Measurement Quantum Cellular Automata and Anomalies in Floquet Codes (2023), [arXiv:2304.01277](https://arxiv.org/abs/2304.01277) [cond-mat, physics:math-ph, physics:quant-ph].
- [33] J. Sullivan, R. Wen, and A. C. Potter, Floquet codes and phases in twist-defect networks (2023), [arXiv:2303.17664](https://arxiv.org/abs/2303.17664) [cond-mat, physics:quant-ph].
- [34] A. Bauer, Topological error correcting processes from

- fixed-point path integrals, *Quantum* **8**, 1288 (2024), [arXiv:2303.16405](#).
- [35] A. Bauer, Low-overhead non-Clifford topological fault-tolerant circuits for all non-chiral abelian topological phases (2024), [arXiv:2403.12119](#) [cond-mat, physics:quant-ph].
- [36] A. Townsend-Teague, J. Magdalena De La Fuente, and M. S. Kesselring, Floquetifying the Colour Code, *Electronic Proceedings in Theoretical Computer Science* **384**, 265 (2023), [arXiv:2307.11136](#) [math-ph, physics:quant-ph].
- [37] H. Bombin, D. Litinski, N. Nickerson, F. Pastawski, and S. Roberts, Unifying flavors of fault tolerance with the ZX calculus, *Quantum* **8**, 1379 (2024).
- [38] V. Motamarri, C. McLauchlan, and B. Béri, SymTFT out of equilibrium: From time crystals to braided drives and Floquet codes (2024), [arXiv:2312.17176](#) [cond-mat, physics:hep-th, physics:quant-ph].
- [39] A. C. Potter and T. Morimoto, Dynamically enriched topological orders in driven two-dimensional systems, *Physical Review B* **95**, 155126 (2017).
- [40] H. C. Po, L. Fidkowski, A. Vishwanath, and A. C. Potter, Radical chiral Floquet phases in a periodically driven Kitaev model and beyond, *Physical Review B* **96**, 245116 (2017).
- [41] D. Aasen, J. Haah, P. Bonderson, Z. Wang, and M. Hastings, Fault-Tolerant Hastings-Haah Codes in the Presence of Dead Qubits (2023), [arXiv:2307.03715](#) [quant-ph].
- [42] C. McLauchlan, G. P. Gehér, and A. E. Moylett, Accommodating Fabrication Defects on Floquet Codes with Minimal Hardware Requirements (2024), [arXiv:2405.15854](#) [quant-ph].
- [43] D. Vu, A. Lavasani, J. Y. Lee, and M. P. A. Fisher, Stable Measurement-Induced Floquet Enriched Topological Order, *Physical Review Letters* **132**, 070401 (2024), [arXiv:2303.01533](#) [cond-mat, physics:quant-ph].
- [44] A. Sriram, T. Rakovszky, V. Khemani, and M. Ippoliti, Topology, criticality, and dynamically generated qubits in a stochastic measurement-only Kitaev model, *Physical Review B* **108**, 094304 (2023), [arXiv:2207.07096](#) [cond-mat, physics:quant-ph].
- [45] Y. Li, X. Chen, and M. P. A. Fisher, Quantum Zeno effect and the many-body entanglement transition, *Physical Review B* **98**, 205136 (2018).
- [46] Y. Li, X. Chen, and M. P. A. Fisher, Measurement-driven entanglement transition in hybrid quantum circuits, *Physical Review B* **100**, 134306 (2019).
- [47] S. Choi, Y. Bao, X.-L. Qi, and E. Altman, Quantum Error Correction in Scrambling Dynamics and Measurement-Induced Phase Transition, *Physical Review Letters* **125**, 030505 (2020).
- [48] C.-M. Jian, Y.-Z. You, R. Vasseur, and A. W. W. Ludwig, Measurement-induced criticality in random quantum circuits, *Physical Review B* **101**, 104302 (2020).
- [49] M. Ippoliti, M. J. Gullans, S. Gopalakrishnan, D. A. Huse, and V. Khemani, Entanglement Phase Transitions in Measurement-Only Dynamics, *Physical Review X* **11**, 011030 (2021).
- [50] M. P. Fisher, V. Khemani, A. Nahum, and S. Vijay, Random Quantum Circuits, *Annual Review of Condensed Matter Physics* **14**, 335 (2023).
- [51] B. Skinner, J. Ruhman, and A. Nahum, Measurement-Induced Phase Transitions in the Dynamics of Entanglement, *Physical Review X* **9**, 031009 (2019).
- [52] Y. Bao, S. Choi, and E. Altman, Theory of the phase transition in random unitary circuits with measurements, *Physical Review B* **101**, 104301 (2020).
- [53] M. Ippoliti and V. Khemani, Postselection-Free Entanglement Dynamics via Spacetime Duality, *Physical Review Letters* **126**, 060501 (2021).
- [54] Y. Li, Y. Zou, P. Glorioso, E. Altman, and M. P. A. Fisher, Cross Entropy Benchmark for Measurement-Induced Phase Transitions, *Physical Review Letters* **130**, 220404 (2023).
- [55] Y. Li and M. P. A. Fisher, Statistical mechanics of quantum error correcting codes, *Physical Review B* **103**, 104306 (2021).
- [56] M. J. Gullans and D. A. Huse, Dynamical Purification Phase Transition Induced by Quantum Measurements, *Physical Review X* **10**, 041020 (2020).
- [57] A. Nahum and B. Skinner, Entanglement and dynamics of diffusion-annihilation processes with Majorana defects, *Physical Review Research* **2**, 023288 (2020).
- [58] A. Nahum, S. Roy, B. Skinner, and J. Ruhman, Measurement and Entanglement Phase Transitions in All-To-All Quantum Circuits, on Quantum Trees, and in Landau-Ginsburg Theory, *PRX Quantum* **2**, 010352 (2021).
- [59] A. Zabalo, M. J. Gullans, J. H. Wilson, S. Gopalakrishnan, D. A. Huse, and J. H. Pixley, Critical properties of the measurement-induced transition in random quantum circuits, *Physical Review B* **101**, 060301 (2020).
- [60] G. M. Sommers, D. A. Huse, and M. J. Gullans, Dynamically generated concatenated codes and their phase diagrams (2024), [arXiv:2409.13801](#) [cond-mat, physics:quant-ph].
- [61] J. Behrends, F. Venn, and B. Béri, Surface codes, quantum circuits, and entanglement phases, *Physical Review Research* **6**, 013137 (2024).
- [62] F. A. Bais and J. K. Slingerland, Condensate-induced transitions between topologically ordered phases, *Physical Review B* **79**, 045316 (2009).
- [63] I. S. Eliëns, J. C. Romers, and F. A. Bais, Diagrammatics for Bose condensation in anyon theories, *Physical Review B* **90**, 195130 (2014).
- [64] Y. Hu, Z. Huang, L.-Y. Hung, and Y. Wan, Anyon condensation: Coherent states, symmetry enriched topological phases, Goldstone theorem, and dynamical rearrangement of symmetry, *Journal of High Energy Physics* **2022**, 26 (2022).
- [65] T. D. Ellison, Y.-A. Chen, A. Dua, W. Shirley, N. Tantiwasadakarn, and D. J. Williamson, Pauli topological subsystem codes from Abelian anyon theories, *Quantum* **7**, 1137 (2023).
- [66] L. Kong, Anyon condensation and tensor categories, *Nuclear Physics B* **886**, 436 (2014).
- [67] F. A. Bais, J. K. Slingerland, and S. M. Haaker, Theory of Topological Edges and Domain Walls, *Physical Review Letters* **102**, 220403 (2009).
- [68] H. Bombin and M. A. Martin-Delgado, Topological Quantum Distillation, *Physical Review Letters* **97**, 180501 (2006).
- [69] H. Bombín, Gauge color codes: Optimal transversal gates and gauge fixing in topological stabilizer codes, *New Journal of Physics* **17**, 083002 (2015).
- [70] M. S. Kesselring, F. Pastawski, J. Eisert, and B. J. Brown, The boundaries and twist defects of the color code and their applications to topological quantum computation, *Quantum* **2**, 101 (2018).

- [71] B. Yoshida, Topological color code and symmetry-protected topological phases, *Physical Review B* **91**, 245131 (2015).
- [72] H. Bombín, G. Duclos-Cianci, and D. Poulin, Universal topological phase of two-dimensional stabilizer codes, *New Journal of Physics* **14**, 073048 (2012).
- [73] A. Kubica, B. Yoshida, and F. Pastawski, Unfolding the color code, *New Journal of Physics* **17**, 083026 (2015).
- [74] J. Haah, Classification of translation invariant topological Pauli stabilizer codes for prime dimensional qudits on two-dimensional lattices, *Journal of Mathematical Physics* **62**, 012201 (2021).
- [75] S. H. Simon, *Topological Quantum* (Oxford University Press, Oxford, United Kingdom, 2023).
- [76] N. D. Mermin, Simple unified form for the major no-hidden-variables theorems, *Physical Review Letters* **65**, 3373 (1990).
- [77] A. Peres, Two simple proofs of the Kochen-Specker theorem, *Journal of Physics A: Mathematical and General* **24**, L175 (1991).
- [78] F. Burnell, Anyon Condensation and Its Applications, *Annual Review of Condensed Matter Physics* **9**, 307 (2018).
- [79] D. Gottesman, The Heisenberg Representation of Quantum Computers, in *Proceedings of the XXII International Colloquium on Group Theoretical Methods in Physics*, edited by S. P. Corney, R. Delbourgo, and P. D. Jarvis (International Press, Cambridge, MA, 1998) pp. 32–43, [arXiv:quant-ph/9807006](https://arxiv.org/abs/quant-ph/9807006).
- [80] H. Bombin, Topological Order with a Twist: Ising Anyons from an Abelian Model, *Physical Review Letters* **105**, 030403 (2010), [arXiv:1004.1838](https://arxiv.org/abs/1004.1838).
- [81] M. Barkeshli, P. Bonderson, M. Cheng, and Z. Wang, Symmetry fractionalization, defects, and gauging of topological phases, *Physical Review B* **100**, 115147 (2019).
- [82] D. Stauffer and A. Aharony, *Introduction to Percolation Theory*, rev. 2. ed., transferred to digital print ed. (Taylor & Francis, London, 2003).
- [83] M. F. Sykes and J. W. Essam, Exact Critical Percolation Probabilities for Site and Bond Problems in Two Dimensions, *Journal of Mathematical Physics* **5**, 1117 (1964).
- [84] S. Krastanov, `QuantumClifford.jl`, <https://github.com/QuantumSavory/QuantumClifford.jl> (2024).
- [85] S. Aaronson and D. Gottesman, Improved simulation of stabilizer circuits, *Physical Review A* **70**, 052328 (2004).
- [86] D. Fattal, T. S. Cubitt, Y. Yamamoto, S. Bravyi, and I. L. Chuang, Entanglement in the stabilizer formalism (2004), [arXiv:quant-ph/0406168](https://arxiv.org/abs/quant-ph/0406168).
- [87] M. A. Nielsen and I. L. Chuang, *Quantum Computation and Quantum Information*, 10th ed. (Cambridge University Press, Cambridge ; New York, 2010).
- [88] A. Lavasani, Y. Alavirad, and M. Barkeshli, Measurement-induced topological entanglement transitions in symmetric random quantum circuits, *Nature Physics* **17**, 342 (2021), [arXiv:2004.07243](https://arxiv.org/abs/2004.07243) [cond-mat, physics:quant-ph].
- [89] F. Venn, J. Behrends, and B. Béri, Coherent-Error Threshold for Surface Codes from Majorana Delocalization, *Physical Review Letters* **131**, 060603 (2023).
- [90] T. Botzung, M. Buchhold, S. Diehl, and M. Müller, Robustness and measurement-induced percolation of the surface code (2023), [arXiv:2311.14338](https://arxiv.org/abs/2311.14338) [cond-mat, physics:quant-ph].
- [91] Y. Zhao and Y. Wan, Nonabelian Anyon Condensation in 2+1d topological orders: A String-Net Model Realization (2024), [arXiv:2409.05852](https://arxiv.org/abs/2409.05852) [cond-mat, physics:hep-th, physics:math-ph].
- [92] Z. Zhang, D. Aasen, and S. Vijay, X-cube Floquet code: A dynamical quantum error correcting code with a subextensive number of logical qubits, *Physical Review B* **108**, 205116 (2023).
- [93] J. F. Humphreys, *A Course in Group Theory*, Oxford Science Publications (Oxford University Press, Oxford; New York, 1996).